3 Biotech (2025) 15:357
https://doi.org/10.1007/s13205-025-04530-z

ORIGINAL ARTICLE

Discovery of platelet glycoprotein VI receptor antagonists and their neuroprotective activity: an in silico, in vitro, and in vivo study

Mohammad Aquib Siddiqui[1] · Poorvi Saraf[2] · Sushant Kumar Shrivastava[2] · Sudha Madhavi Penumaka[3] · Debabrata Mandal[3] · Ravi Saini[4] · Abhishek Pathak[5] · Kakarla Ramakrishna[6] · Sairam Krishnamurthy[1]

Received: 14 May 2025 / Accepted: 7 September 2025 / Published online: 21 September 2025

Abstract

The present study utilized a drug repurposing approach to identify potential GPVI receptor antagonists among FDA-approved drugs. Computational and molecular dynamics simulations revealed that adapalene and ranolazine exhibit strong binding affinities to GPVI receptors and stabilize GPVI proteins, respectively. Both compounds inhibited collagen-induced platelet aggregation, evidenced by the suppression of Syk tyrosine kinase expression, a marker of platelet activation, via GPVI stimulation, as confirmed through flow cytometry analysis. Further analysis using circular dichroism and Raman spectroscopy indicated that collagen exposure induced conformational changes in the α-helical domains of platelets, which were stabilized upon treatment with adapalene and ranolazine. Moreover, thrombotic events can lead to cerebral cell death due to hypoxia, which may be mitigated by neuroprotective compounds. Adapalene and ranolazine were assessed for their neuroprotective capabilities. The results showed that these compounds exhibited neuroprotective effects in SHSY5Y neuroblastoma cells subjected to oxygen–glucose deprivation/reperfusion (OGD/R) injury, reducing HIF-1α expression, ROS production, lipid peroxidation, and caspase-3 levels, while also improving mitochondrial membrane potential and glutathione levels. Acridine orange and propidium iodide staining studies further confirmed a decrease in apoptosis. In the $FeCl_3$-induced carotid artery thrombosis model, ranolazine effectively inhibited platelet aggregation by modulating GPVI receptor activity, reducing intracellular calcium levels, and enhancing cAMP signaling. It also suppressed critical platelet activation mediators, including COX-1, TXB_2, and PGE_2, thereby mitigating thrombus formation. Collectively, these results suggest that adapalene and ranolazine may serve as multimodal therapeutic agents with the potential to treat both thrombotic and neurological diseases. Future studies focusing on the adapalene and ranolazine molecular mechanisms, bleeding risk, dose titration, and long-term safety while managing thrombotic disorders have to be investigated.

Keywords Adapalene · Ranolazine · Drug repurposing · GPVI receptor · Neuroprotection

Introduction

Thrombotic disorders account for a considerable number of deaths globally and contribute to increasing rates of morbidity (Asada et al. 2018). Thrombosis is a process of the formation of clots, which constitute a set of conditions characterized by the development of thrombi within the vasculature, which can result in significant and sometimes life-threatening conditions. Further, various long-term health conditions such as diabetes, specific autoimmune and autoinflammatory disorders, and several types of cancer are also linked to a heightened likelihood of developing thrombotic disorders (Duffett 2022; Pastori et al. 2023; Vaidya et al. 2021). Moreover, thrombotic events also contribute to the development of cerebrovascular diseases, which account for approximately 33% of mortality in developed nations worldwide (Benjamin et al. 2018).

To mitigate and manage thrombotic disorders, strategies that target the suppression of platelet activation and their aggregation are of fundamental importance. Several antiplatelet drugs have been approved for the treatment of platelet-related thrombotic diseases. Indeed, these therapies have undesirable side effects such as hemorrhage (including gastrointestinal and cerebral bleeding), low white blood cell count, headache, skin inflammation, and high blood pressure (Taylor et al. 2014). Moreover, the recombinant tissue plasminogen activator (rtPA) is the only effective thrombolytic agent with a limited therapeutic window after stroke onset

Extended author information available on the last page of the article

and is also contraindicated in hemorrhagic strokes, which emphasizes the direct need for novel, potential, and safe antiplatelet agents (Chapman et al. 2014; Shibata et al. 2022). Therefore, exploring platelet receptors that inhibit the initial cascade of platelet activation, platelet aggregation, and thrombus formation could provide better therapeutic interventions for thrombotic illnesses such as cerebral stroke.

Glycoprotein VI (GPVI), present on platelets, plays a vital role in platelet aggregation. Collagen interacts with and stimulates GPVI, activating Src-family kinases, which then activate the immunoreceptor tyrosine-based activation motif (ITAM) (Makhoul et al. 2019a). This recruits spleen tyrosine kinase (Syk), which activates phospholipase Cγ2, leading to increased inositol trisphosphate (InsP3) and calcium levels, which eventually release platelet activation mediators, leading to platelet activation and aggregation (Makhoul et al. 2019a). Therefore, altering the interaction between collagen and GPVI receptors may present a possible strategy for decreasing platelet aggregation and preventing thrombus formation.

A recent analysis of GPVI-Fc fusion proteins and humanized murine GPVI scFvs highlighted the potential of GPVI as a therapeutic target (Taylor et al. 2014). GPVI-Fc fusion proteins demonstrate the suppressed collagen reactions without adverse effects in animal studies, and individuals deficient in GPVI do not exhibit a significant predisposition to excessive bleeding (Al-Tamimi et al. 2012; Beck et al. 2023; Vismara 2021). These findings support the rationale of targeting the collagen–GPVI interaction as a means to inhibit thrombus formation without substantially increasing the risk of hemorrhage. Moreover, several candidate drugs are currently undergoing clinical trials in phases I and II (Revacept-fusion protein and ACT017-antibody), but thus far, no GPVI receptor small molecule antagonist has been approved for commercial use (Jourdi et al. 2021). Moreover, people experiencing a severe acute ischemic stroke involving large blood vessels have substantial neuronal degeneration and neurological decline (Saver 2006; Shen et al. 2023; Huang et al. 2023). Therefore, agents that not only inhibit platelet aggregation but also inhibit cellular apoptosis contribute significantly to the management of cerebral stroke (Yeung and Holinstat 2012; Gresele and Momi 2022b).

In addition, recent findings suggest that Losartan, an angiotensinogen II receptor antagonist, has been reported to suppress collagen-induced platelet aggregation and block the clustering of the glycoprotein VI receptor, without affecting the binding of collagen (Onselaer et al. 2020). Hence, compounds that specifically target GPVI could have significant therapeutic benefits in combating thrombotic events. Drug repurposing encompasses the identification of innovative therapeutic applications for existing drugs, potentially reducing the time, cost, and risk of traditional drug development (Roy et al. 2021). In recent times, drug repurposing has gained significant attention in drug discovery, particularly in the prevention and treatment of thrombotic diseases (Yeung and Holinstat 2012; Gresele and Momi 2022a). Hence, given the importance of the need for novel, safe, and efficacious treatment requirements for combating thrombotic diseases.

Adapalene, an FDA-approved topical retinoid, modulates cell turnover and reduces inflammation, which helps prevent the formation of acne lesions (Rusu et al. 2020). On the other hand, ranolazine, which is primarily approved for the treatment of chronic angina, works by improving blood flow and inhibiting late sodium currents, thereby reducing the oxygen demand of the heart muscle (Aldakkak et al. 2013). In the present study, we have performed the drug repurposing approach and identified adapalene and ranolazine as the most potent GPVI inhibitors to combat thrombotic diseases through four main objectives. First, computational methods, including in silico screening followed by molecular docking and dynamics simulations, were used to screen ligands for GPVI affinity. Second, the antiplatelet activity of selected ligands was assessed in vitro, examining Syk tyrosine kinase levels and blood clotting times, alongside protein–ligand interaction stability via spectroscopic techniques. Third, the neuroprotective effects of compounds against oxygen–glucose deprivation/reperfusion injury in neuroblastoma cells were evaluated by assessing cell viability, mitochondrial function, oxidative stress, and apoptosis. Fourth, an in vivo ferric chloride-induced carotid artery thrombosis model was utilized to analyze ranolazine's effects on platelet–ligand interactions, GPVI levels, calcium signaling, aggregation, and oxidative stress markers.

Materials and methods

Reagents and chemicals

Adapalene (ADA) (TCI, CAS no: 106685–40-9), ranolazine (RAN) (Sigma Aldrich, CAS no: 95635–55-5), clopidogrel (CLOP) (Dr. Reddy's, India), fibrinogen (Himedia), tirofiban (TIR) (TCI chemicals), losartan (Karnataka antibiotics and pharmaceutical ltd., India), dabigatran etexilate (Disto Pharma, India), adenosine diphosphate (ADP) (CAS no: 16178–48-6, Sigma Aldrich, USA), thrombin (CAS no: 9002044, Sigma Aldrich, USA), collagen (Sigma Aldrich, CAS no: 9007–34-5), SH-SY5Y cell line (NCCS, Pune), Dulbecco's modified Eagle's medium/F12 (DMEM/F12), DMEM (glucose-free), fetal bovine serum, HBSS, and 0.25% Trypsin–EDTA (Gibco), MTT (TCI chemicals), dimethyl sulfoxide (DMSO) (TCI chemicals), dichlorodihydrofluorescein diacetate (DCFHDA, Sigma, CAS no: 4091990), HIF-1α (KBH0422 Krishgen Biosystems, India), sGPVI (BHE15208612, biohippo), cyclic adenosine monophosphate (K11-0299, KinesisDx), thromboxane B_2

(501,020, Cayman Chemical), cyclooxygenase 1 (K11-0909, KinesisDx), prostaglandin E_2 (KLR0504, Krishgen Biosystems), Syk polyclonal antibody (BS-0685R, Thermo Fisher Scientific), caspase-3 (KBH4804, Krishgen Biosystems), and MitoRed (sc-301164, Chem Cruz) were procured. The Amplex Red kit (A22188) was purchased from Thermo Fisher for the estimation of H_2O_2. All supplementary reagents and chemical compounds utilized in this study were procured from local vendors.

Animals

Male Wistar rats (250–300 g) were procured from the central animal facility at the Institute of Medical Sciences (IMS), Banaras Hindu University (BHU), Varanasi-221005, India. The rats were kept in standard laboratory settings with unrestricted accessibility to water and food, and a regular light–dark schedule. Prior to commencing the study, permission was granted from the Institutional Animal Ethics Committee (IAEC Approval number—IIT (BHU)/IAEC/2023/027). A 2-week adaptation time was given to all test animals before the experiments commenced. All experimental protocols were conducted according to the CCSEA guidelines, India and regulations specified in the National Institutes of Health Guide for Laboratory Animal Care and Use.

Experimental design

The current study included four experimental objectives. The first set of objective is focused on computational studies to screen and identify the affinity of ligands for GPVI receptors. This involved in-depth molecular modeling and simulation to predict the interactions between ligands and receptors using molecular docking and molecular dynamics simulation studies. The second objective was to assess the antiplatelet activity of the screened ligands in terms of in vitro platelet aggregation activity and to estimate the level of Syk tyrosine kinase, a marker for GPVI receptor activation, via flow cytometry. Further, in vitro blood clotting time was estimated to assess the safety profile and anticoagulant efficacy of the screened compounds. This objective also involves the assessment of the stability of protein–ligand interactions through circular dichroism and Raman spectroscopy techniques. For the third objective, the neuroprotective effects of the selected compounds were screened against oxygen–glucose deprivation/reperfusion (OGD/R) injury in neuroblastoma SHSY5Y cell lines. This involved a comprehensive set of assays such as the MTT assay, mitochondrial membrane potential (MMP), hypoxia-inducible factor-1α (HIF-1α), reactive oxygen species (ROS), malondialdehyde (MDA), glutathione (GSH), acridine orange and propidium iodide staining, and caspase-3 level measurements. The fourth objective included an in vivo ferric chloride-induced carotid artery thrombosis model to estimate platelet–ligand binding interaction using isothermal titration calorimetry, platelet GPVI levels, platelet calcium levels using flow cytometry, biomarkers of platelet aggregation, and platelet oxidative stress. In this objective, only ranolazine was selected, as adapalene demonstrated very low bioavailability following oral administration (Piskin and Uzunali 2007; Aura et al. 2020). Therefore, this involved randomly selected male Wistar rats (200–250 g), allocated to the respective groups: group 1: Sham control, group 2: $FeCl_3$ only, group 3: $FeCl_3$ + RAN 15 mg/kg, group 4: $FeCl_3$ + RAN 30 mg/kg, group 5: $FeCl_3$ + RAN 60 mg/kg, and group 6: $FeCl_3$ + CLOP 40 mg/kg or $FeCl_3$ + Losartan 25 mg/kg. The doses of ranolazine (Williams et al. 2014), clopidogrel (Paul et al. 2023), and losartan (Murad et al. 2012) were determined based on prior research findings. The experimental design of the $FeCl_3$-induced thrombosis model was adapted from prior established methodologies (Ramakrishna et al. 2022a).

In silico computational study

Molecular modeling or virtual screening

A combined approach using virtual screening was utilized to identify potential candidates from a group of FDA-approved drugs. This method employs both molecular docking and Prime/MM-GBSA modeling techniques (Genheden and Ryde 2015). The DrugBank provided a total of 2369 FDA-approved drugs for this study. Initially, the existing libraries were evaluated via the high-throughput computational screening mode of Glide. Those molecules that demonstrated excellent performance (with a docking score of ≤ -7) were subsequently filtered through the standard precision docking mode. The hit molecules with potential (score ≤ -8) from the SP docking data were subsequently further analyzed via the extraprecision docking mode. Results of XP docking were subsequently screened using an XP GScore equal to or less than -9 (Arora et al. 2019). Molecules with an XP G score below -9.0 from the docking procedure were further analyzed through Prime/MM-GBSA calculations. Molecules with a binding free energy (B.E.) of less than -9.0 kcal/mol were subsequently advanced to the next screening step. The subsequent filtration involved conducting molecular dynamics simulations to evaluate the stability and structural robustness of the docked molecular assemblies (Kumar et al. 2022; Zhou et al. 2020).

Molecular docking method The molecular docking analyses of the compounds were conducted using the "Glide" module of the Schrodinger Maestro 2018.1 platform. The protein X-ray crystal structure of glycoprotein VI (pdb:

2GI7) underwent preprocessing, correction, and refinement via the "Protein preparation wizard" module of the Schrodinger software. A grid ($10\times10\times10$ Å^3) was generated around the active site of the protein and further validated by re-docking the bound ligand into the generated grid, using the grid generation wizard. The binding groove of GPVI was found to be formed by a variety of essential amino acids (AA) residues, including Lys41, Ser43, Ser44, Gln48, Gln50, Leu53, Phe54, Pro56, Lys59, Arg60, Ser61, Leu62, Arg66, Tyr66, Val34, Leu3, Trp76, Arg38, and Glu40, present within the collagen-binding domain of GPVI receptor (Horii et al. 2006; Feitsma et al. 2022). The ligands were prepared using the "Ligprep" module, and the "Glide XP" module of Schrodinger was employed to perform the docking studies. The compound losartan was utilized as a reference standard in the study because of its known inhibition of the GPVI receptor protein (Onselaer et al. 2020). The binding interactions of the ligands within the active sites of the protein were examined utilizing the Schrodinger Maestro 2018.1 (Singh et al. 2022).

Molecular dynamics (MD) Following the molecular docking process, the docked complexes of ligands with GPVI were subjected to MD simulations via the Desmond module of the Schrodinger Maestro 2018.1. Initially, a tool was utilized to construct a simulation system based on a TI3P model. The docked complex was enclosed within a cubic box, and an algorithm for simulated annealing with 5000 iterations and a convergence limit of 1.0 kcal/mol/Å was then implemented to lower the energy of the system. The production run consisted of simulating over 100 ns (ns), and the resulting trajectories were examined via a protocol for simulating interactions (Saraf et al. 2022).

In vitro platelet study

Platelet-rich plasma (PRP) isolation The blood samples were obtained from rats using the retro-orbital plexus technique, which underwent centrifugation at 1000 rpm and 37 ºC for 10 min to isolate the platelet-rich plasma (PRP). Platelet-poor plasma (PPP) was obtained at 3000 rpm at 37 ºC for 10 min from the remaining blood after extracting the PRP. The platelets were subsequently separated from the PRP at 350 g for 10 min, and the platelet concentration was then normalized to 4×10^8 cells/ml using Tyrode's solution (Ramakrishna et al. 2022a).

Platelet aggregation method The in vitro antiplatelet activity of the test compounds, in combination with losartan, clopidogrel, and dabigatran, was evaluated via a 96-well plate aggregometry method (Cheng et al. 2020). Initially, PRP (200 µl) was incubated with varying doses of adapalene, ranolazine (5, 10, and 20 µM), losartan (10 µM), clopidogrel (30 µM) (Wu et al. 2020b), and dabigatran (10 µM) in different sets of experiments. The absorbance of the 96-well plate at 570 nm was quantified via the SpectraMax M5 microplate reader. Further, platelet-aggregating agonists, either collagen (5 µg/ml), ADP (10 µM), or thrombin (0.05 U/ml) were introduced to induce platelet aggregation at 37 ºC for 5 min. Absorbance measurements were obtained at 570 nm via a microplate spectrophotometer (SpectraMax M5, USA) (Ramakrishna et al. 2022a). The IC_{50} of adapalene and ranolazine against collagen, ADP, and thrombin-mediated platelet aggregation were assessed via nonlinear regression analysis with GraphPad Prism 8. The optical density of the PPP was utilized as a blank, from which the percentage of platelet aggregation was subsequently derived as

$$\begin{aligned} Plateletaggregationrate\% = {} & PRP(beforestimulationabs) \\ & - PRP(afterstimulationabs) \times 100 \\ & \div PRP(beforestimulationabs) - PPPabs \end{aligned}$$

Fibrinogen-induced platelet aggregation method The antiplatelet activity of tirofiban in comparison to adapalene and ranolazine was assessed via a 96-well plate aggregometry technique (Cheng et al. 2020). The objective of this study was to compare the screened compounds with marketed tirofiban for the rapid inhibitory effect on platelet aggregation over an equivalent time period, independent of the mechanism of action. The PRP (200 µl) was initially exposed to varying concentrations of tirofiban (5, 10, and 20 µM). The absorbance taken at a wavelength of 570 nm was quantified via a multiwell plate reader (SpectraMax M5, USA). Subsequently, a platelet-aggregating agonist, fibrinogen (0.2 mg/ml), was introduced to induce platelet aggregation at 37 ºC for 5 min, with a few modifications (Zimran and Elstein 2003; Ciborowski and Tomasiak 2009).

Flow cytometric assessment of the platelet Syk tyrosine kinase The platelets were isolated and processed via a methodology previously outlined in the literature with certain modifications (Ramakrishna et al. 2022a; Harper et al. 2013). The platelets were exposed to various concentrations of adapalene, ranolazine, losartan, and clopidogrel for a period of 10 min at 37 °C before being stimulated with 5 µg/ml collagen for a period of 20 min. Upon activation and permeabilization, the platelets were exposed to a phospho-Syk polyclonal primary antibody (1:50) for 20 min at ambient temperature. The samples were then exposed to FITC-labeled secondary antibody for a duration of 1 h at ambient temperature. Later, the cells were stabilized with a 2% PFA solution. After fixation, permeabilization, and labeling with antibodies, the platelets were analyzed within 2 h via a flow cytometer (CytoFLEX, Beckman, USA), and the acquired data were subjected to analysis utilizing the FlowJo soft-

ware (V10) (Feldman et al. 2008) (Li et al. 2020; Jiang et al. 2015; Kundalevich et al. 2024).

Estimation of the stability of platelet–ligand interactions via circular dichroism (CD) and Raman spectroscopy The conformational alterations in platelets exposed to collagen (5 µg/ml) and the screened compounds (20 µM), as well as the stability of platelet–ligand binding interaction, were further verified via CD (CD Polarimeter J-1500, JASCO, Japan) and Raman spectroscopy (WITec alpha300, Germany) techniques, which aligned with a previously reported method with some modifications (Tripathi et al. 2023). Spectroscopic measurements were used to analyze the integrity of the protein's secondary structure, including alpha-helices, beta-sheets, and random coils, utilizing the BESTSEL web tool and Origin software (v6.0) (Marchelak et al. 2023; Tripathi et al. 2023; Kharazian et al. 2018; Kundalevich et al. 2024).

In vitro clotting assay PRP was obtained as previously described (Ramakrishna et al. 2022a) and incubated with test compounds at 37 ℃ for 1 min. Clot formation was induced by adding 0.25 M $CaCl_2$, and the time to visible clot formation was estimated. Control experiments used a saline (0.9% NaCl) solution (Liu et al. 2015).

In vitro cell line study

The oxygen–glucose deprivation/reoxygenation (OGD/R) model To study cerebral ischemic injury in SHSY5Y neuroblastoma cell lines, an oxygen–glucose deprivation/reoxygenation (OGD/R) model was utilized (Alluri et al. 2015; Juntunen et al. 2020). Cells were cultured at 37 °C in DMEM/F12 supplemented with 10% fetal bovine serum, penicillin (50 U/ml), streptomycin (100 µg/ml), and 10 µM retinoic acid. Cultures were maintained in a humidified incubator with 5% CO2 and 95% air mixture. The cells were subsequently subjected to varying concentrations of adapalene and ranolazine (5 µM, 10 µM, and 20 µM) for 12 h before the induction of OGD/R (Lin et al. 2021). The cells were subsequently grown in a glucose-free medium without fetal bovine serum under oxygen and glucose-deficient (OGD) conditions for 4 h, as previously described (Zhang et al. 2019). Subsequently, cells were transferred to a normoxic setting and provided with a normal culture medium for reoxygenation. Control samples were incubated in high-glucose DMEM/F12 for 24 h (Lin et al. 2021; Zhang et al. 2019).

Assay for cell viability and neurotoxicity Cell viability was assessed using the MTT assay, which relies on reducing 3-(4,5-dimethylthiazol-2-yl)-2,5-diphenyltetrazolium bromide. Cells, seeded at 5.0×10^3 cells/well, were incubated overnight before exposure to varying compound concentrations following an OGD/R treatment (test compounds dissolved in DMSO were added to culture media at concentrations not exceeding 1%, ensuring no adverse effects on cell viability). After a 4-h incubation with MTT solution at 37 °C, absorbance was measured at 550 nm using a microplate spectrophotometer (Lin et al. 2021; Tripathi et al. 2023).

Mitochondrial membrane potential (MMP) assay MMP changes were assessed using MitoTracker Red staining (Kashyap et al. 2023). Following exposure to the test compounds and OGD/R, the cells were incubated with MitoTracker Red in basal DMEM for 40 min at 37 °C, washed with phosphate-buffered saline (PBS), and then imaged using a ZEISS Cell Discoverer 7 (Carl Zeiss, Germany) microscope at 10X magnification (Rele et al. 2024).

Quantification of HIF-1α in SHSY5Y cells A quantitative sandwich ELISA immunoassay kit (Krishgen Biosystems) was used. Lysates from SHSY5Y cells in all the experimental groups after exposure to test compounds and OGD/R were prepared, and the level of HIF-1α was quantified at 400 nm via a microtiter plate spectrophotometer (SpectraMax M5, USA) (Song et al. 2018; Tambuwala et al. 2019; Gervin et al. 2020).

Quantification of ROS, MDA, and GSH content in SHSY5Y cells After drug and OGD/R treatment, cells were washed, incubated with 10 µM DCF-DA in the dark for 30 min, and measured using a fluorescence microplate reader at 490/520 nm (Tripathi et al. 2023; Lin et al. 2021). The lipid peroxidation end product, malondialdehyde, in neuroblastoma SHSY5Y cells was quantified (UĞUZ et al. 2015). Further, glutathione levels in SHSY5Y cells were measured by spectrophotometry at 412 nm (UĞUZ et al. 2015; Nazıroğlu et al. 2019).

Acridine orange (AO) and propidium iodide (PI) staining in SHSY5Y cells After the cells had been subjected to the test compounds and OGD/R, the cells underwent incubation with 10 µg/ml AO/PI for 5 min in the dark at a temperature of 37 °C. The cells were subsequently examined under a ZEISS Cell Discoverer 7 (Carl Zeiss, Germany) microscope at 10X magnification (Yu et al. 2018; Amar et al. 2023).

Estimation of Caspase-3 level in SHSY5Y cells Following exposure to the test compounds and OGD/R, the cell supernatants were processed based on the manufacturer's protocol, and absorbance was measured at 450 nm using a microtiter plate spectrophotometer (SpectraMax M5, USA) (Tudor et al. 2021).

In vivo $FeCl_3$-induced carotid artery thrombosis model

For this in vivo model, only ranolazine was chosen, as adapalene exhibits poor bioavailability following oral administration (Piskin and Uzunali 2007; Aura et al. 2020). RAN and CLOP were dissolved in 0.5% DMSO and orally administered for 1 week. Following the final dose, the rats were anesthetized with thiopentone sodium (40 mg/kg) after a 30-min interval. The right common carotid artery was carefully isolated, and a presoaked Whatman filter paper containing ferric chloride was applied to the CCA for 5 min. The filter paper was then removed, and the CCA was washed with normal saline to mitigate the potential effects of $FeCl_3$ on the surrounding tissues (Ramakrishna et al. 2022a). Furthermore, the study quantified platelet–ligand interaction using ITC, platelet soluble GPVI, cyclic adenosine monophosphate, and plasma levels of TXB_2, COX-1, and PGE_2 using ELISA techniques. In addition, platelet reactive oxygen species, hydrogen peroxide, and NOX-1 levels were measured according to established methodologies (Ramakrishna et al. 2022a).

Isothermal titration calorimetry (ITC) Platelets were isolated and processed according to a previously reported methodology (Ramakrishna et al. 2022a). A calorimetric analysis was performed with a few modifications to quantify the binding affinity between ranolazine and activated as well as resting or non-activated platelet samples. This experiment utilized a MicroCal PEAQ-ITC (Malvern panalytical) maintained at a temperature of 25 °C. Titration analyses were conducted by sequentially injecting 2 µl aliquots (except the first injection had 0.4 µl) of a 20 µM ranolazine solution into a sample cell containing 270 µl activated platelets [5 µg/ml collagen for 5 min (Ramakrishna et al. 2022a)], with rapid mixing at 750 rpm; the procedure involved 19 injections at 150 s intervals until near-saturation was attained. The calorimetric binding constant K_D for each injection was determined after accounting for the heat released upon dilution of the platelets, which was measured and calculated using MicroCal PEAQ-ITC Control software (Assumpção et al. 2010; Zimran and Elstein 2003).

Quantification of platelet soluble GPVI receptor levels Plasma samples were obtained from various experimental groups, and the levels of soluble GPVI were quantified through an ELISA Kit in accordance with the manufacturer's protocol.

Quantification of intracellular calcium levels in platelets using flow cytometry The washed platelets were treated with the fluorescent dye Fura-2AM (5 µM). The labeled platelets were maintained at room temperature for 30 min in the dark. Thereafter, intracellular calcium mobilization was observed for 2 min by flow cytometer (CytoFLEX, Beckman, USA) following incubation with the ranolazine (5, 10, and 20 µM) and subsequent exposure to collagen (5 µg/ml) (Gillespie et al. 2018; Makhoul et al. 2019b).

Measurement of biomarkers of platelet aggregation Plasma concentrations of COX-1, thromboxane B_2, prostaglandin E_2, and platelet cyclic adenosine monophosphate were quantified utilizing ELISA kits in accordance with the manufacturer's specified procedures.

Measurement of platelets' oxidative stress Platelet ROS concentrations were quantified via the fluorescent probe dichlorodihydrofluorescein diacetate. Platelets were treated with DCFHDA (10 µM) in the dark for 30 min at 37 °C, and absorbance was estimated at 485/520 nm. In addition, platelet hydrogen peroxide levels were assessed employing an Amplex Red assay kit (Liu et al. 2019). The NOX-1 concentration was also determined using an ELISA kit (Krishgen Biosystems).

Statistical analysis

Statistical analysis was performed using GraphPad Prism8. Data are presented as mean ± standard deviation. One-way ANOVA followed by Tukey's test was used for comparisons and post hoc analysis, respectively. IC_{50} values for adapalene and ranolazine against collagen were determined by nonlinear regression analysis. Significance was determined at $p < 0.05$.

Results

In silico computational study

In silico virtual screening

The crystal structure of GPVI was utilized for molecular docking with Glide in XP mode. The virtual screening of all 2369 FDA-approved drugs was conducted via a validated grid. Molecules with XP GScore values < -9.0 kcal/mol were identified to ensure diversity for the subsequent screening stage. The binding free energies of the protein–ligand docked complexes were subsequently estimated via the Prime MM-GBSA approach, enabling rapid ranking of a large set of ligands and generating more reliable results while eliminating false positives. After the high-throughput virtual screening mode of Glide was used, 1162 compounds were filtered out from a total of 2369 compounds obtained from FDA-approved drugs (Drug Bank). Further filtering in standard precision docking mode resulted in the identification of 221 ligands, and subsequent extraprecision docking

mode narrowed the selection to 82 compounds. Among these, 82 compounds were predicted to exhibit binding free energies below -9.0 kcal/mol. A further evaluation was subsequently conducted on the remaining 82 compounds via the MM-GBSA methodology to estimate the binding free energy. The threshold criterion for the binding free energy (dG) was fixed at -90 kcal/mol (Zhou et al. 2020). Ultimately, four ligands with dG values lower than this threshold were successfully identified after comprehensive analysis [Fig. 1]. Further, the objective of the research was to determine the structural stability, perform a comprehensive evaluation of the interactions of GPVI with four specific molecules, and calculate the average binding free energy via MD simulations across a trajectory snapshot. Four potential compounds, namely adapalene, ranolazine, azilsartan, and lapatinib, which are complexed with GPVI, were chosen for examination via MD simulations.

Molecular docking study

In this study, we repurposed the aforementioned four drugs as GPVI modulators with the help of docking studies. The docking scores were as follows: adapalene scored -10.15 kcal/mol, ranolazine scored -9.68 kcal/mol, azilsartan scored -9.43 kcal/mol, lapatinib scored -9.01 kcal/mol, and losartan scored -7.45 kcal/mol when docked with GPVI. The docking score reflects the binding energy, where lower values indicate a stronger affinity of the drug for the receptor. Figure 2 depicts the interaction of ligands with the receptor, whereas Table 1 displays both the binding free energy and the amino acid residues that interact with the receptor active site and are essential for interaction and receptor activation. Our findings indicate that compared with losartan, adapalene, ranolazine, azilsartan, and lapatinib are more likely to interact with the collagen-binding domain of the glycoprotein VI receptor.

Molecular dynamics simulation

MD simulations of adapalene on GPVI indicated the stability of the docked pose of the adapalene–GPVI complex. The 100-ns simulation revealed that adapalene interacted with the key amino acid residues within the GPVI active binding groove. The protein–ligand RMSD value of the simulated trajectory reached a maximum of 2.9 Å. The RMSD (root mean square deviation) value of the simulated trajectory

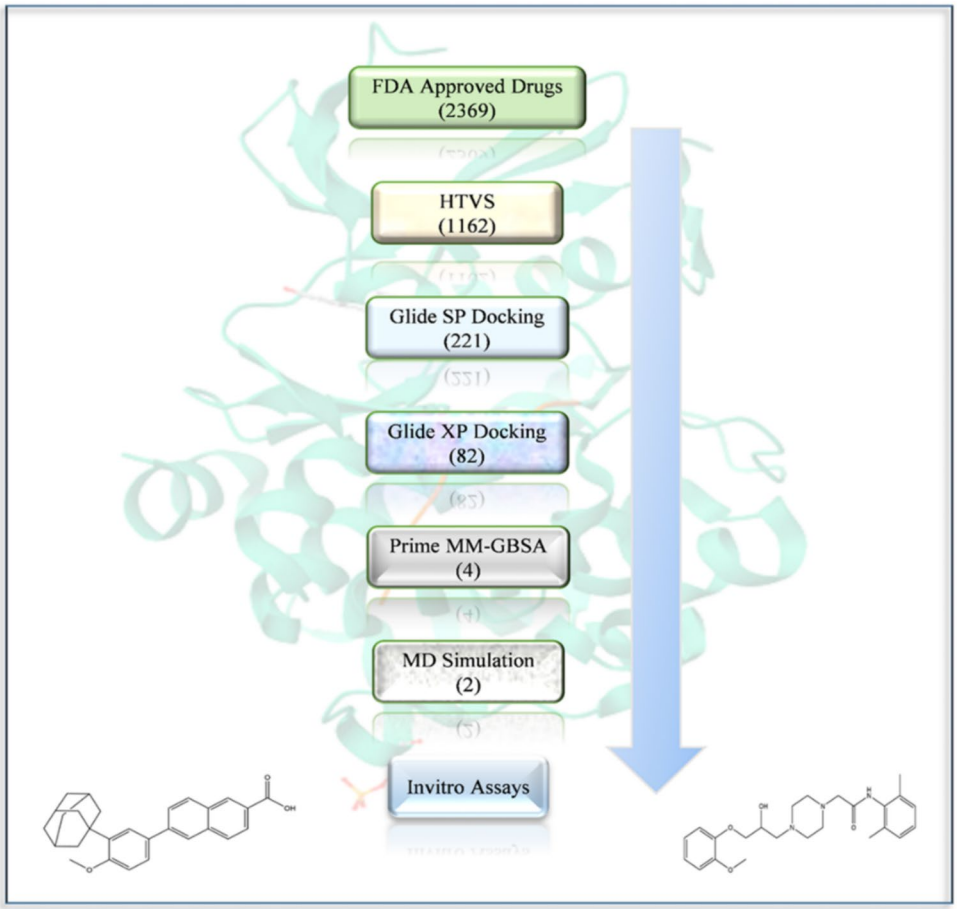

Fig. 1 Docking-based virtual screening workflow

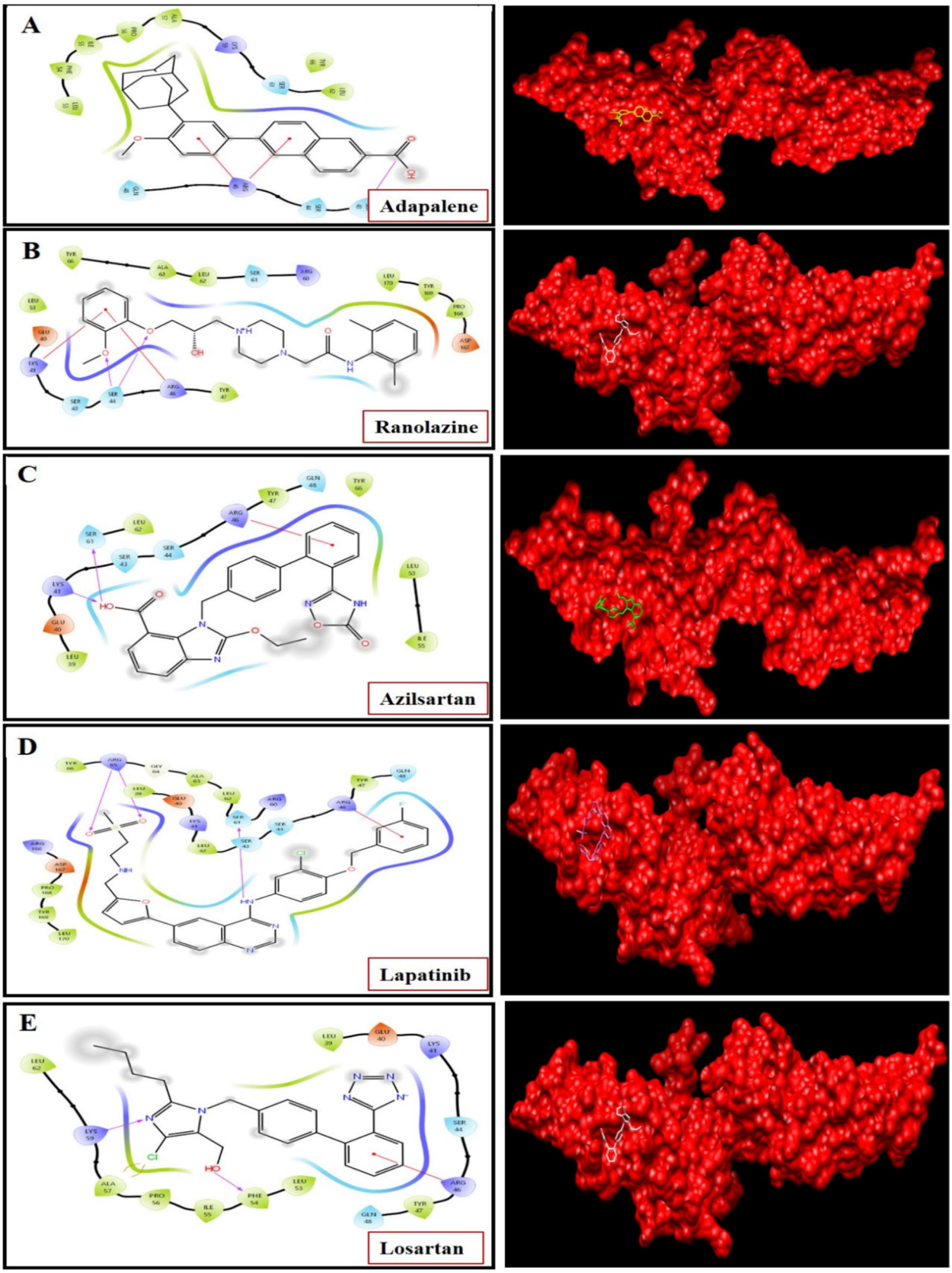

Fig. 2 Computed structural analysis and binding characteristics (visualization accomplished with Schrodinger Maestro 2018.1 (column I) and UCSF Chimera (column II)) of adapalene (**A**), ranolazine (**B**), azilsartan (**C**), lapatinib (**D**), and losartan (**E**) with the GPVI receptor

Table 1 Computational docking results of adapalene, ranolazine, azilsartan, lapatinib, and losartan with the GPVI receptor

S. no	Compound	B.E (kcal/mol)	Interacting amino acids
1	Adapalene	− 10.15	Lys41, Ser43, Ser44, Gln48, Leu53, Phe54, Pro56, Lys59, Ser61, Leu62, Tyr66
2	Ranolazine	− 9.68	Lys41, Ser43, Ser44, Leu53, Arg60, Ser61, Leu62, Tyr66, Glu40
3	Azilsartan	− 9.43	Lys41, Ser43, Ser44, Gln48, Leu53, Ser61, Leu62, Tyr66, Glu40
4	Lapatinib	− 9.01	Lys41, Ser43, Ser44, Gln48, Arg60, Ser61, Leu62, Tyr66, Glu40
5	Losartan	− 7.45	Lys41, Ser44, Gln48, Leu53, Phe54, Pro56, Lys59, Leu62, Glu40

was within the acceptable range of 1–3 Å. The adapalene displayed prominent interactions with the amino acid residues Lys41, which is primarily involved in collagen binding (Taylor et al. 2014). Adapalene has also shown hydrophobic interactions with the key residues of the binding groove, e.g., Leu53, Pro56, and Leu62. In addition, other key amino acid residues, Gln50 and Ser61, showed polar interaction with adapalene. In addition, the interactions observed in the docking study persisted throughout the simulation run [Fig. 3].

Furthermore, MD simulations for ranolazine were also executed for a duration of 100 ns to establish the stability of the GPVI–ranolazine complex. The protein–ligand RMSD value of the simulated trajectory reached a maximum of 3.0 Å, which was within the acceptable range of 1–3 Å. The results showed that ranolazine significantly interacted with the key AA residues of the GPVI active binding groove. Ranolazine interacted with the essential amino acid residue Lys41, resulting in charged interactions and Pi–cation interactions. Ranolazine also showed strong hydrophobic interactions with residues Leu53, Phe54, Pro56, and Tyr66, which are responsible for the overall stability of the GPVI–ranolazine complex. In addition, other key amino acid residues, Gln48 and Ser44, showed polar interaction with ranolazine. Ranolazine and GPVI residues were stable throughout the 100-ns simulation run [Fig. 4].

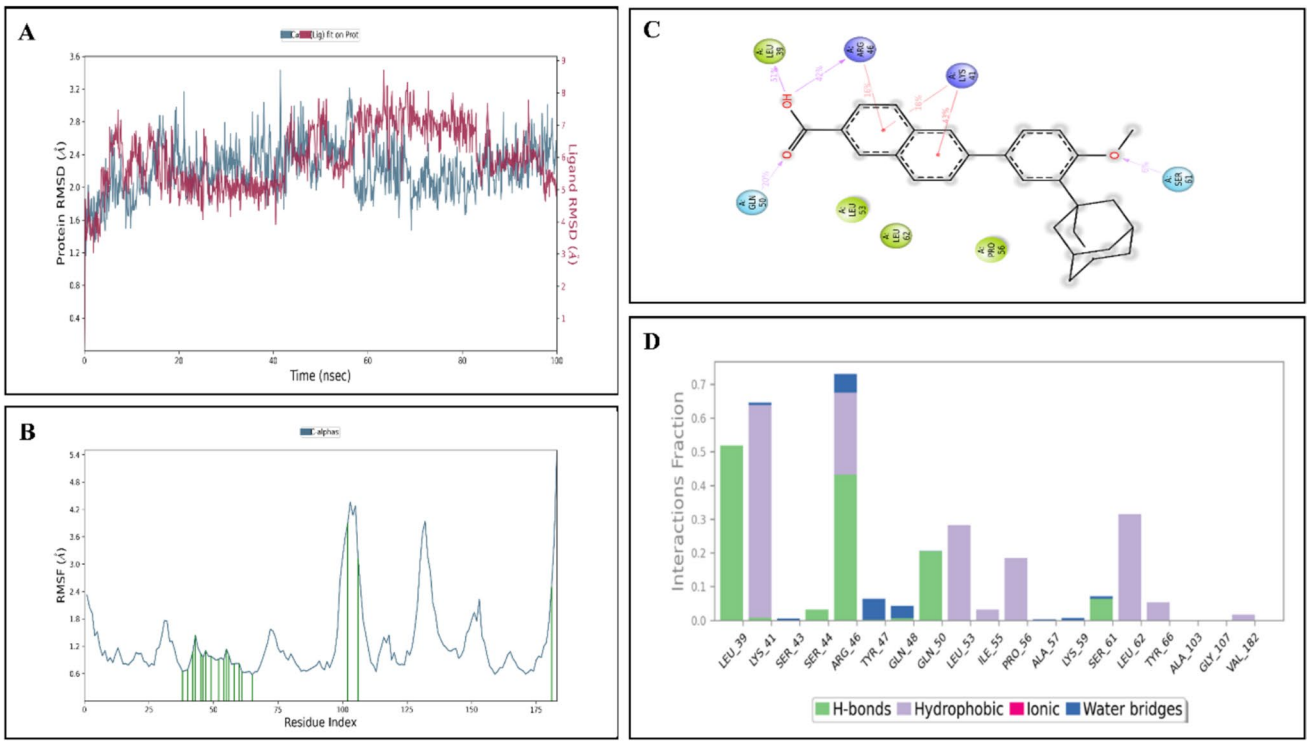

Fig. 3 MD simulation of the adapalene–GPVI docked complex: **A** RMSD graph of adapalene during a 100 ns run; **B** RMSF plot of protein; **C** 2D depiction of the interaction with AA residues in the active site; **D** histogram showing protein interaction with ligand

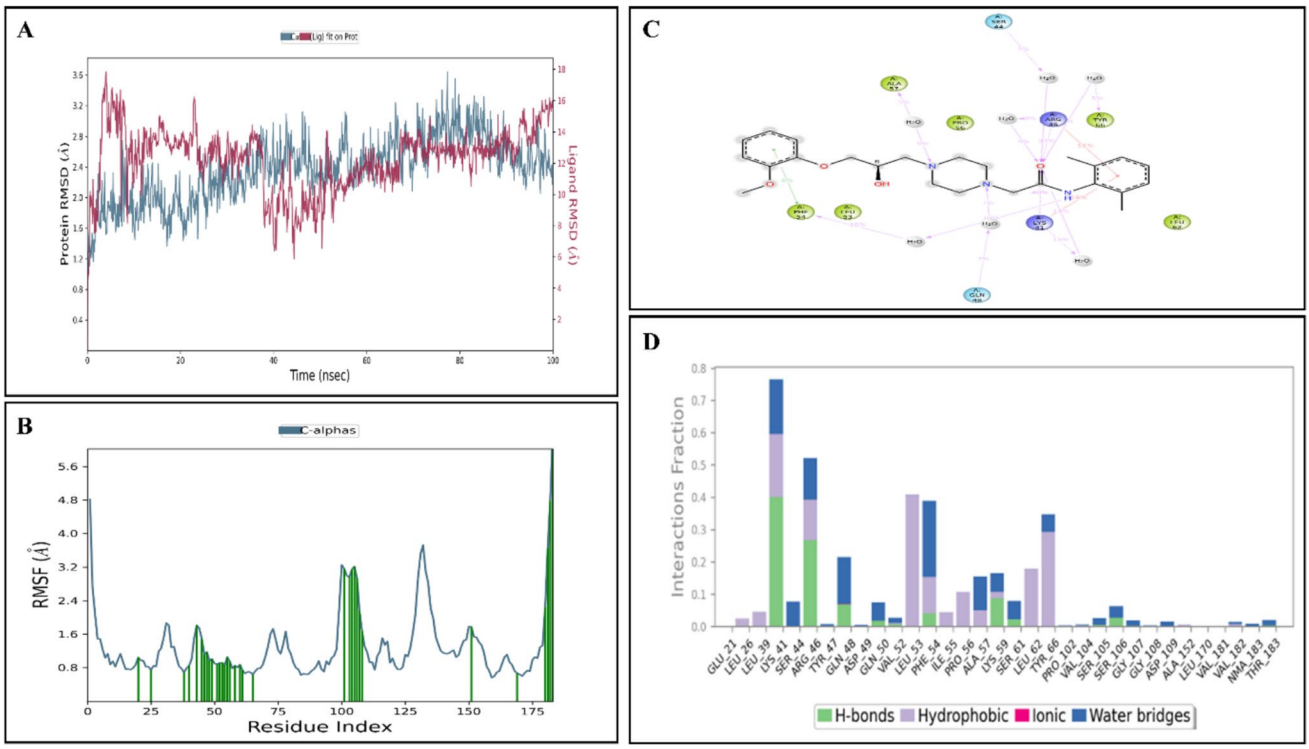

Fig. 4 MD simulation of the ranolazine–GPVI docked complex: **A** RMSD graph of ranolazine during the 100 ns run; **B** RMSF plot of protein; **C** 2D depiction of interaction with AA residues in the active site; **D** histogram showing protein interaction with ligand

In vitro platelet study

Adapalene and ranolazine inhibited the in vitro platelet aggregation

Figure 5A and 5B displays the half-maximal inhibitory concentrations (IC_{50}) of adapalene and ranolazine in relation to platelet aggregation, whereas Fig. 5C illustrates their inhibitory effects on in vitro platelet aggregation. One-way ANOVA analysis depicted significant variations among the groups: collagen [$F(7, 40) = 129.3$; $P < 0.0001$], ADP [$F(7, 40) = 8.017$; $P < 0.0001$], and thrombin [$F(7, 40) = 99.38$; $P < 0.0001$]. The IC_{50} values for adapalene and ranolazine were determined as 11.51 ± 2.5 µM, [CI (95%) = 12.003] and 15.47 ± 3.7 µM, [CI (95%) = 16.115] against collagen-mediated platelet aggregation, respectively. Post hoc tests revealed that treatment with adapalene or ranolazine results in a concentration-dependent decrease in the percentage of collagen-induced platelet aggregation. It is important to note that no significant differences were observed among the adapalene 20 µM, ranolazine 20 µM, and Losartan 10 µM treated groups. In the case of ADP and thrombin-induced platelet aggregation, no significant differences were observed among the ADP/Thrombin, adapalene, and ranolazine-treated groups [Fig. 5D, 5E]. These findings indicate that both drugs exert antiplatelet activities through inhibiting the collagen-induced platelet aggregation, but not through the inhibition of ADP and thrombin-dependent mechanisms.

Adapalene and ranolazine demonstrated superior and rapid inhibition of in vitro platelet aggregation compared to the marketed compound tirofiban

A one-way ANOVA analysis demonstrated significant variations in platelet aggregation across the different groups: [$F(8, 45) = 86.15$; $P < 0.0001$]. During the identical incubation period, it was noted that adapalene 20 µM and ranolazine 20 µM led to a decrease in collagen-induced platelet aggregation by approximately 14.83% and 17.4%, respectively. Conversely, tirofiban 20 µM demonstrated inhibition of platelet aggregation up to around 27.58% when incubated with fibrinogen for the same duration. In addition, the 20 µM tirofiban treatment group demonstrated a statistically significant variation in comparison to the 20 µM adapalene and 20 µM ranolazine treatment groups [Fig. 5F]. The findings demonstrate that adapalene and ranolazine exhibit a more rapid inhibitory effect on platelet aggregation compared to tirofiban.

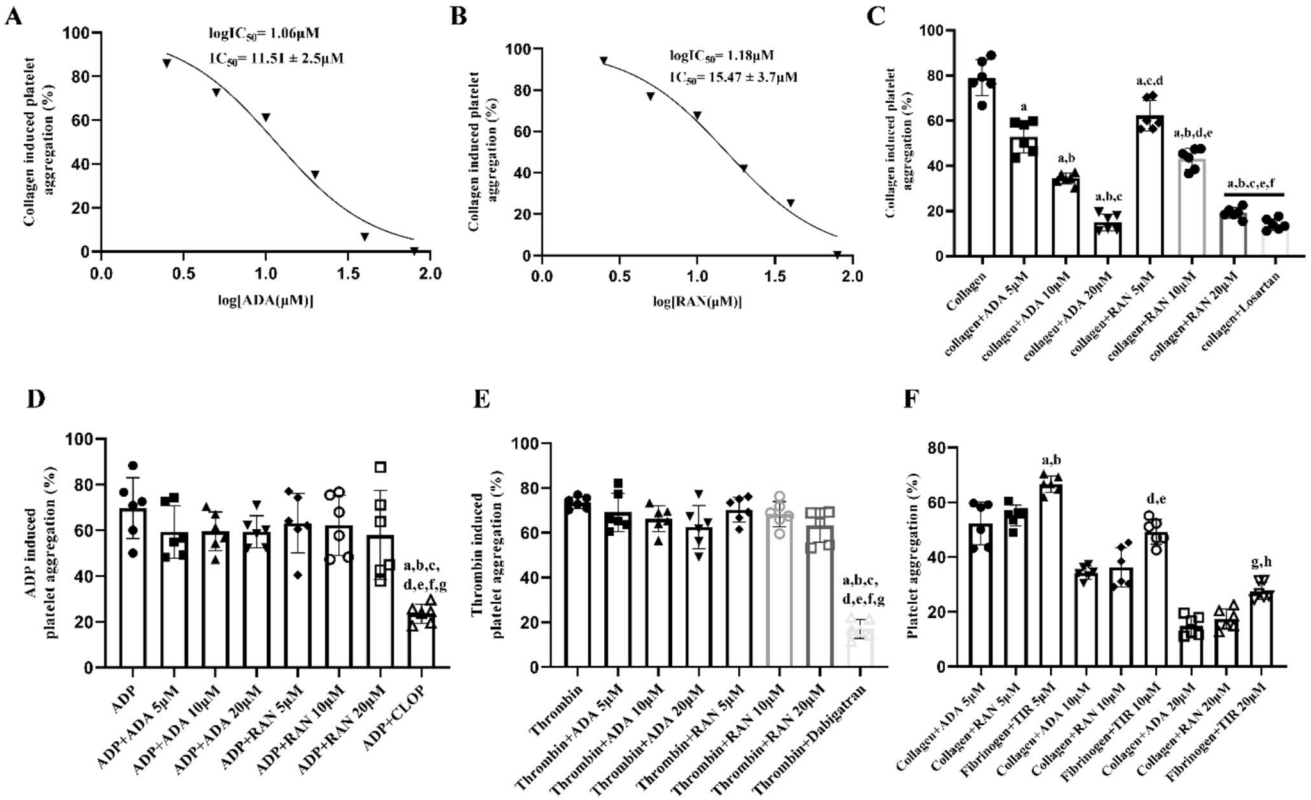

Fig. 5 **A**, **B** IC_{50} of adapalene and ranolazine against collagen-induced platelet aggregation. **C** Adapalene and ranolazine ameliorated the collagen-induced platelet aggregation. **D** Adapalene and ranolazine showed no effect on ADP-induced platelet aggregation. **E** Adapalene and ranolazine showed no effect on thrombin-induced platelet aggregation. $^{a}p<0.05$ compared to collagen/ADP/Thrombin, $^{b}p<0.05$ compared to collagen/ADP/Thrombin + 5 μM ADA, $^{c}p<0.05$ compared to collagen/ADP/Thrombin + 10 μM ADA, $^{d}p<0.05$ compared to collagen/ADP/Thrombin + 20 μM ADA, $^{e}p<0.05$ compared to collagen/ADP/Thrombin + 5 μM RAN, $^{f}p<0.05$ compared to collagen/ADP/Thrombin + 10 μM RAN, and $^{g}p<0.05$ compared to collagen/ADP/Thrombin + 20 μM RAN in their respective groups. All values are represented in the form of mean ± SD ($n=6$). (One-way ANOVA followed by Tukey's multiple comparison post hoc test). **F** Comparative activity of adapalene, ranolazine, and tirofiban (temporal study) on platelet aggregation. $^{a}p<0.05$ compared to collagen + 5 μM ADA, $^{b}p<0.05$ compared to collagen + 5 μM RAN, $^{c}p<0.05$ compared to fibrinogen + 5 μM Tirofiban, $^{d}p<0.05$ compared to collagen + 10 μM ADA, $^{e}p<0.05$ compared to collagen + 10 μM RAN, $^{f}p<0.05$ compared to fibrinogen + 10 μM tirofiban, $^{g}p<0.05$ compared to collagen + 20 μM ADA, and $^{h}p<0.05$ compared to collagen + 20 μM RAN in their respective groups. All values are represented in the form of mean ± SD ($n=6$). (One-way ANOVA followed by Tukey's multiple comparison post hoc test)

Adapalene and ranolazine mitigated Syk tyrosine kinase level

The one-way ANOVA demonstrated statistically significant differences among groups [F (7, 16) = 74.17; $p<0.0001$]. Subsequent analysis revealed that treatment with adapalene and ranolazine led to a substantial reduction in Syk protein expression compared to the collagen-treated group [Fig. 6]. No substantial differences were observed between ADA 20 μM, RAN 20 μM, and Losartan 10 μM, respectively. Following collagen induction, Syk phosphorylation levels increased by 17 ± 0.61%. However, in comparison to the treatment groups, those treated with adapalene and ranolazine demonstrated a dose-dependent decrease in Syk tyrosine kinase level, particularly at 20 μM (3.68 ± 0.59% and 4.1 ± 1.2%), respectively. Treatment with 30 μM clopidogrel exhibited a statistically non-significant difference in comparison to the collagen-treated group.

Estimation of platelet–ligand interaction stability

Spectroscopic data were acquired from 3 sets of experiments: untreated platelets, platelets activated solely by collagen, and platelets that were first exposed to adapalene and ranolazine and then to collagen.

The circular dichroism (CD) spectrum of activated platelets treated with test compounds displayed an α-helix band, together with two negative bands around 209 nm and 222 nm. The content was found to be 28.52 ± 0.13%. However, when the platelets were treated solely with collagen, this percentage decreased to 4.63 ± 0.17%, suggesting that the conformation and structures of the platelets had been

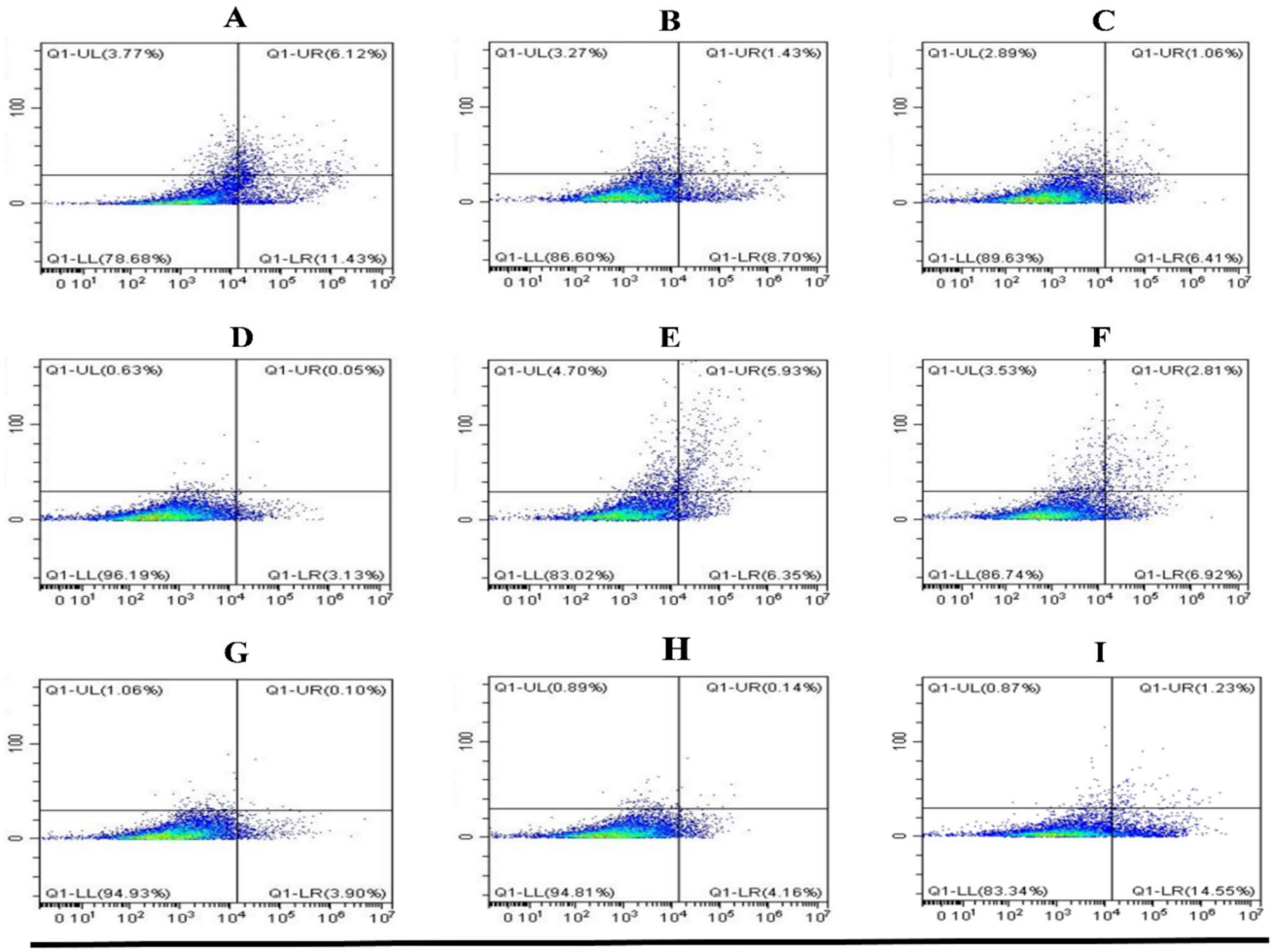

Fig. 6 Adapalene and ranolazine treatment reduces SYK tyrosine kinase phosphorylation. A. Collagen, B. collagen + ADA5 μM, C. collagen + ADA10 μM, D. collagen + ADA20 μM, E. collagen + RAN5 μM, F. collagen + RAN10 μM, G. collagen + RAN20 μM, H. collagen + losartan10 μM, and I. collagen + CLOP30 μM. [a]$p < 0.05$ compared to collagen, [b]$p < 0.05$ compared to collagen + 5 μM ADA, [c]$p < 0.05$ compared to collagen + 10 μM ADA, [d]$p < 0.05$ compared to collagen + 20 μM ADA, [e]$p < 0.05$ compared to collagen + 5 μM RAN, [f]$p < 0.05$ compared to collagen + 10 μM RAN, [g]$p < 0.05$ compared to collagen + 20 μM RAN, and [h]$p < 0.05$ compared to collagen + 10 μM Losartan in their respective groups. All values are represented in the form of mean ± SD ($n = 3$). (One-way ANOVA followed by Tukey's multiple comparison post hoc test)

altered [Fig. 7A]. Raman spectroscopic analysis depicted a shift in the amide I band within the α-helix region of platelets treated solely with collagen. In addition, spectroscopic analysis also revealed that the ligands or test compounds interacted with the carbonyl (C = O) groups of the protein subunits, as evidenced by a shift in the position of the amide I peak compared to the spectra of activated platelets. The findings revealed that platelets remained stable following treatment with the two test compounds. Furthermore, Raman spectra for the selected compounds were computed using the Gaussian software program across the wavenumber range of 0 to 4000 cm^{-1}. Following this, a linear scaling procedure was applied to the wavenumber data within the fingerprint region of 600–2000 cm^{-1}. The obtained spectra were analyzed through a review of relevant scientific literature (Zyubin et al. 2020). The majority of the reported frequencies were derived from experimental observations. The 1001 cm^{-1} vibration is associated with the experimental band of the aromatic ring in phenylalanine. Examination of the 800–950 cm^{-1} region revealed various spectral differences among the groups under investigation. They generally describe the vibrational characteristics of the aromatic groups present in the amino acids tyrosine and phenylalanine when exposed to selected compounds. The region from 941 to 955 cm^{-1} exhibited vibrational modes of the carbon–carbon backbone, while the 1154 cm^{-1} peak indicated carbon–carbon bond stretching, and the 1450 cm^{-1} peak demonstrated bending of the methylene (CH_2) groups. The observed changes in spectral intensity and frequency shifts during therapy are correlated with the theoretically calculated vibrational modes. Spectroscopic analysis revealed that shifts at 1339 cm^{-1} and 814 cm^{-1} were associated with aromatic compounds. The 1666 cm^{-1} band was found to be proximal to the experimentally observed Amide I band. In addition, the 1621 cm^{-1} band characterized hydrogen bonding in the complex and may serve as potential biomarkers for therapeutic response. Consequently, we observed that ligands binding to the collagen-binding sites stabilized the platelets before they underwent denaturation via collagen, as indicated by the spectral data [Fig. 7B]. This study was supported by our findings from molecular dynamics (MD) simulations and in vitro experiments, which demonstrated that the test compounds stably interacted with the collagen-binding site of platelets and inhibited their activation and aggregation processes.

Adapalene and ranolazine prolong the in vitro blood clotting

In order to examine the test compounds anticoagulant activity, the in vitro clotting time was examined. One-way analysis of variance depicted that significant variations were observed between the groups: [$F(7, 24) = 64.31$; $P < 0.0001$]. Post hoc assessment indicated that exposure to adapalene and ranolazine results in a concentration-dependent increase in clotting time, indicating the anticoagulant

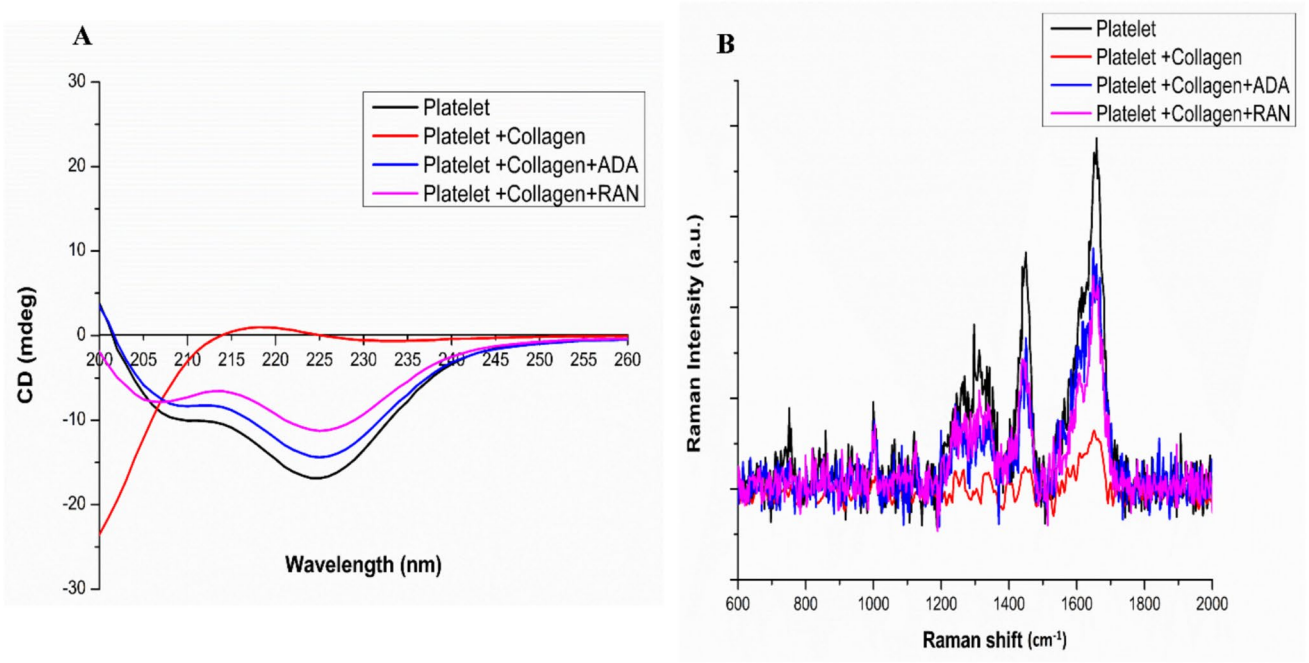

Fig. 7 Adapalene and ranolazine showed structural stabilization of platelets by inhibiting platelet aggregation. **A** CD and **B** Raman spectra of the resting platelets and platelets in the presence and absence of collagen, adapalene (20 µM), and ranolazine (20 µM)

activity of the compounds. Moreover, the administration of adapalene at a concentration of 20 µM, and ranolazine 20 µM, showed a significant difference with clopidogrel 30 µM [Fig. 8A]. The results suggest that the test compounds may have a protective effect by not excessively prolonging clotting time, indicating an absence of substantial procoagulant activity. Furthermore, after 2 h of clot formation, it has been observed that low-dose treated clots are dense and firm, whereas clots treated with a high dose of test compounds appear to be less compact and lighter [Fig. 8B]. Hence, the screened compounds were shown to have anticoagulant effects, suggesting that both compounds can also be used as antithrombotic agents.

Cell line study

Neurotoxicity assay

The MTT (3-(4,5-dimethylthiazol-2-yl)-2,5-diphenyltetrazolium bromide) colorimetric method was employed to examine the neurotoxic nature of both compounds. Exposure of cells to varying concentrations of adapalene and ranolazine did not show a significant effect [one-way ANOVA tests were conducted, with F (6, 21) = 21.95; $p < 0.0001$, Fig. 9A, F (6, 21) = 15.82; $p < 0.0001$, Fig. 9B] on the viability of SHSY5Y cells in comparison to the control group upto 40 µM. Therefore, for further studies, concentrations of both test compounds used in the pharmacological study were adjusted to 5, 10, and 20 µM as these compound doses are safer for further studies.

Adapalene and ranolazine suppressed OGD/R-induced cellular toxicity in MTT assay

We explored the potential neuroprotective properties of adapalene and ranolazine in a model of OGD/R-induced ischemic cell death utilizing SHSY5Y cells. As a point of comparison, clopidogrel (a widely recognized medication for cerebral ischemia) was employed as a standard reference due to its use in managing ischemic stroke during both the acute phase for aspirin-hypersensitive patients and in the context of long-term secondary prevention measures (Kamarova et al. 2022). One-way ANOVA analysis has shown significant variations in cell viability among the groups [F (8, 27) = 82.89; $P < 0.0001$] [Fig. 9C]. We have observed a significant decrease in SHSY5Y cell viability after OGD/R induction. However, pretreatment with adapalene and ranolazine effectively increased the cell viability in a concentration-dependent manner. Following OGD/R exposure, cell viability decreased by 78.52 ± 10.47% compared to the control group, which had 100% cell viability. Nevertheless, treatment with adapalene and ranolazine at a maximum concentration of 20 µM after exposure to OGD/R proved more effective, significantly enhancing cell viability to 87.43 ± 8.26% and 86.73 ± 7.13%, respectively, when compared to the control group. In addition, clopidogrel

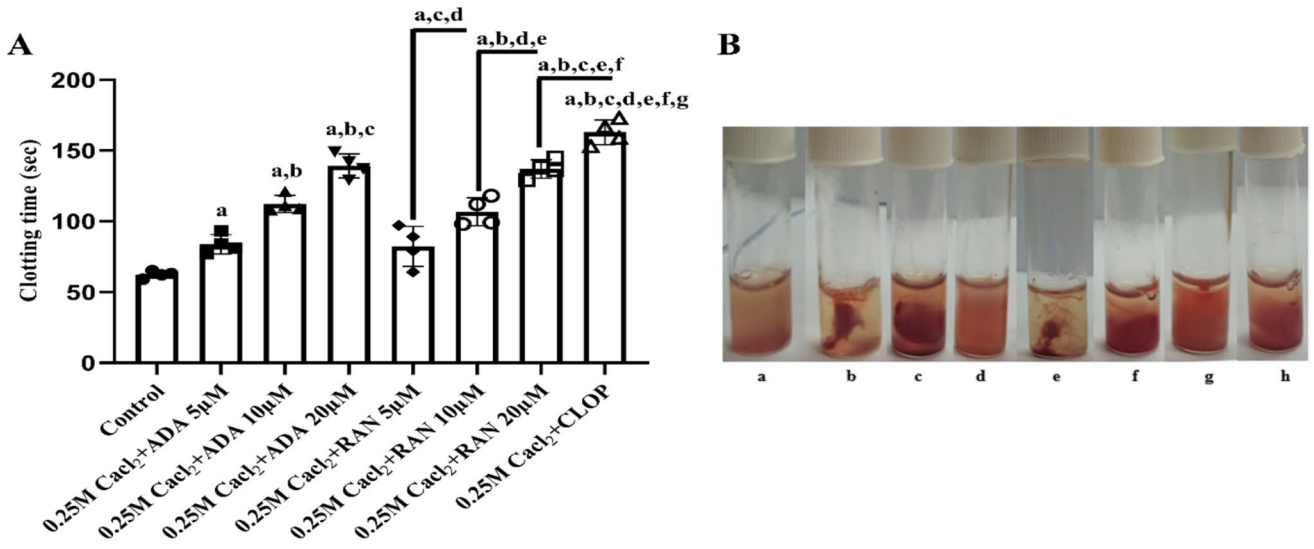

Fig. 8 **A** Adapalene and ranolazine prolonged the clotting time. [a]$p < 0.05$ compared to control, [b]$p < 0.05$ compared to 0.25 M $CaCl_2$ + 5 µM ADA, [c]$p < 0.05$ compared to 0.25 M $CaCl_2$ + 10 µM ADA, [d]$p < 0.05$ compared to 0.25 M $CaCl_2$ + 20 µM ADA, [e]$p < 0.05$ compared to 0.25 M $CaCl_2$ + 5 µM RAN, [f]$p < 0.05$ compared to 0.25 M $CaCl_2$ + 10 µM RAN, and [g]$p < 0.05$ compared to 0.25 M $CaCl_2$ + 20 µM RAN in their respective groups. All values are represented in the form of mean ± SD ($n = 4$). (One-way ANOVA followed by Tukey's multiple comparison post hoc test). **B** Adapalene and ranolazine alleviated the formation of dense clots after 2 h. [A. control, B. 0.25 M $CaCl_2$ + ADA 5 µM, C. 0.25 M $CaCl_2$ + ADA 10 µM, D. 0.25 M $CaCl_2$ + ADA 20 µM, E. 0.25 M $CaCl_2$ + RAN 5 µM, F. 0.25 M $CaCl_2$ + RAN 10 µM, G. 0.25 M $CaCl_2$ + RAN 20 µM, and H. 0.25 M $CaCl_2$ + CLOP 30 µM]

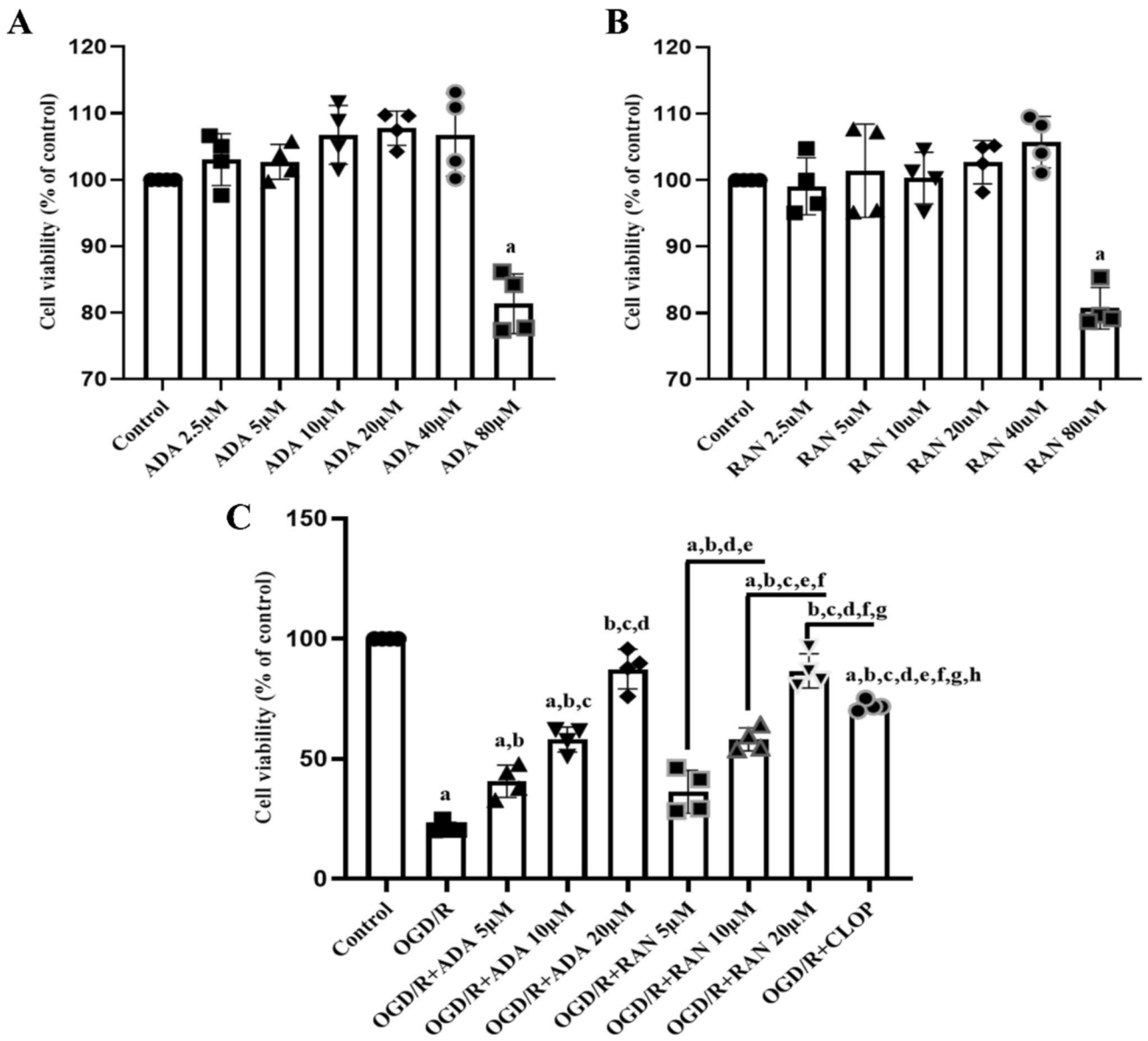

Fig. 9 Study on the neuroprotective effects of the selected compounds on the SHSY5Y cell line. **A**, **B** Cell viability of adapalene and ranolazine on SH-SY5Y cells. **C** Adapalene and ranolazine enhance cell viability in SHSY5Y Cells subjected to OGD/R. $^{a}p<0.05$ compared to control, $^{b}p<0.05$ compared to OGD/R, $^{c}p<0.05$ compared to OGD/R + 5 μM ADA, $^{d}p<0.05$ compared to OGD/R + 10 μM ADA, $^{e}p<0.05$ compared to OGD/R + 20 μM ADA, $^{f}p<0.05$ compared to OGD/R + 5 μM RAN, $^{g}p<0.05$ compared to OGD/R + 10 μM RAN, and.$^{h}p<0.05$ compared to OGD/R + 20 μM RAN in their respective groups. All values are represented in the form of mean ± SD ($n=4$). (One-way ANOVA followed by Tukey's multiple comparison post hoc test)

restored cellular viability to approximately 72.22 ± 2.18% as compared to the control group. These findings indicate that both compounds exhibited significant neuroprotection against OGD/R injury.

Adapalene and ranolazine attenuated OGD/R-induced disruption of mitochondrial membrane potential (Δψm)

We have further evaluated the mitochondrial membrane potential (MMP) using the MitoRed dye in SHSY5Y cells. One-way ANOVA analysis has shown significant variations among the groups: [F (8, 18) = 149.8; $P<0.0001$]. Our results indicate that OGD/R leads to a substantial decline in MMP, with the magnitude of this reduction dependent on the dosage or concentration. In contrast, 20 μM (adapalene and ranolazine) exhibit statistically significant differences with the clopidogrel 30 μM in the post hoc analysis [Fig. 10]. These findings suggest that both drugs exhibited significant cell viability due to preserving MMP after OGD/R injury.

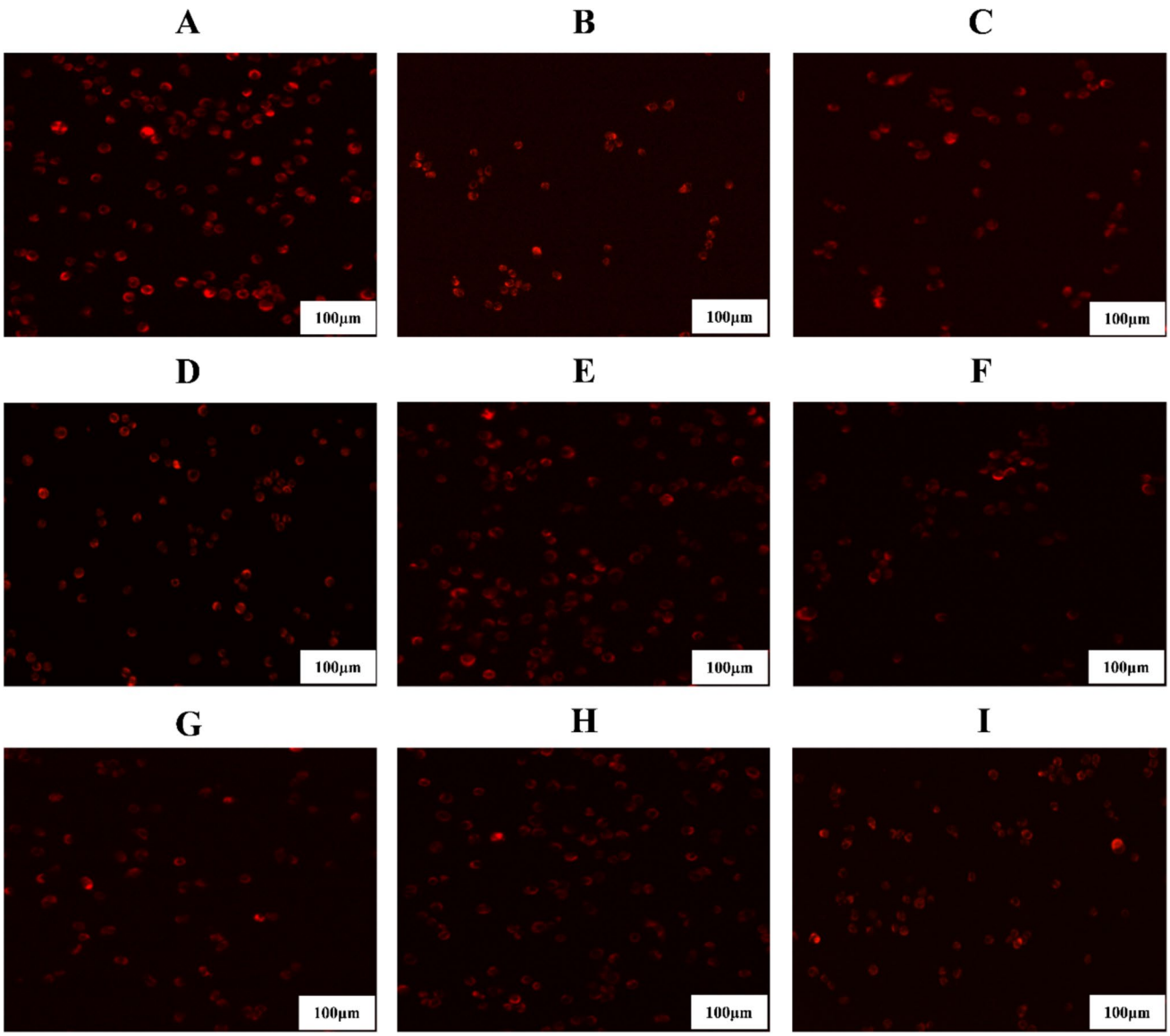
A
B
C
D
E
F
G
H
I
100μm
Fluorescence intensity (a.u.)
150
100
50
0
a
a,b
a,b,c
b,c,d
a,b,d,e
a,b,c,e,f
b,c,d,f,g
a,b,c,e,f,h
Control
OGD/R
OGD/R+ADA 5μM
OGD/R+ADA 10μM
OGD/R+ADA 20μM
OGD/R+RAN 5μM
OGD/R+RAN 10μM
OGD/R+RAN 20μM
OGD/R+CLOP

◂**Fig. 10** Adapalene and ranolazine elevated the MMP of the cells tracked using MitoRed in SHSY5Y cells subjected to OGD/R. **A** control, **B** OGD/R, **C** OGD/R + ADA 5 µM, **D** OGD/R + ADA 10 µM, **E** OGD/R + ADA 20 µM, **F** OGD/R + RAN 5 µM, **G** OGD/R + RAN 10 µM, **H** OGD/R + RAN 20 µM, and **I** OGD/R + CLOP 30 µM. [a]$p < 0.05$ compared to control, [b]$p < 0.05$ compared to OGD/R, [c]$p < 0.05$ compared to OGD/R + 5 µM ADA, [d]$p < 0.05$ compared to OGD/R + 10 µM ADA, [e]$p < 0.05$ compared to OGD/R + 20 µM ADA, [f]$p < 0.05$ compared to OGD/R + 5 µM RAN, [g]$p < 0.05$ compared to OGD/R + 10 µM RAN, and.[h]$p < 0.05$ compared to OGD/R + 20 µM RAN in their respective groups. All values are represented in the form of mean ± SD ($n = 3$). (One-way ANOVA followed by Tukey's multiple comparison post hoc test)

Adapalene and ranolazine alleviated HIF-1α expression

The one-way ANOVA analyses indicated significant differences among the groups [$F(8, 36) = 387.5$; $p < 0.0001$] [Fig. 11A]. There was a significant increase in HIF-1α levels among the OGD/R group in comparison to the control group. Further, the administration of varying concentrations of adapalene and ranolazine (5 µM, 10 µM, and 20 µM) shows a decrease in HIF-1α levels in a concentration-dependent manner, with 20 µM showing greater effectiveness against the OGD/R model. These findings indicate that both compounds reduced the HIF-1α levels, thereby enhancing cell viability.

Adapalene and ranolazine mitigated ROS, MDA, and restored GSH levels

One-way ANOVA analysis showed a significant variation among the groups: ROS [$F(8, 27) = 144.6$; $p < 0.0001$] [Fig. 11B], MDA [$F(8, 36) = 119.8$; $p < 0.0001$] [Fig. 11C], and GSH [$F(8, 36) = 135.0$; $p < 0.0001$] [Fig. 11D]. OGD/R exposure raised ROS levels by 78.55 ± 6.73% compared to the control group. Conversely, the adapalene and ranolazine treatment group exhibited a dose-dependent scavenging of ROS and MDA levels in comparison to the OGD/R group, with 20 µM showing greater efficacy against OGD/R-mediated ischemic cell death. However, the OGD/R group showed notably decreased GSH levels in SHSY5Y cells, while the treatment groups significantly boosted these levels. These results suggested that the increase in cell viability could be due to its antioxidant effects.

Adapalene and ranolazine protects against OGD/R-mediated apoptosis in SHSY5Y cells

The one-way ANOVA analysis for AO/PI dual staining demonstrated a statistically significant variation in the mean outcomes across the experimental groups [$F(8, 18) = 416.2$; $p < 0.0001$]. Exposure to OGD/R elevated apoptosis levels by 77.33 ± 3.05% compared to the control group. In contrast, groups subjected to adapalene and ranolazine exhibited a concentration-dependent reduction in apoptosis relative to the OGD/R group, with the 20 µM concentration demonstrating the most efficacious. Specifically, adapalene 20 µM and ranolazine 20 µM showed significant differences with the clopidogrel 30 µM-treated group [Fig. 12]. These findings suggest that the mitigation of apoptosis by the selected compounds could be the reason for increased cell viability.

Adapalene and ranolazine alleviated caspase-3 level

The one-way ANOVA analyses indicated significant differences among the groups [$F(8, 36) = 273.8$; $p < 0.0001$] [Fig. 13]. The OGD/R group displayed a statistically significant increase in caspase-3 levels when contrasted with the control group. In addition, the administration of adapalene and ranolazine at varying concentrations induced a concentration-dependent decrease in caspase-3 expression, with the 20 µM concentration exhibiting maximal efficacy in the OGD/R model. These observations suggest that the enhanced cell viability may be a consequence of apoptosis reduction mediated by the tested compounds.

In vivo platelet study using $FeCl_3$-induced carotid artery thrombosis model

Ranolazine showed binding affinity with collagen-activated platelets

Isothermal titration calorimetry was employed to perform two experimental studies that validated the binding interaction between ranolazine and the platelets, which was manifested through collagen-induced activation. In the initial experimental set, resting or non-activated platelets were introduced into the sample cell and exposed to 10 µl of ranolazine using a Hamilton syringe. In the second set of experiments, platelets were first pre-incubated with collagen for 5 min, and then this solution was transferred into the sample cell and subsequently treated with 10 µl ranolazine. The isotherm of ranolazine revealed an exothermic interaction with the collagen-activated platelets, exhibiting a binding constant K_D $(1.52 \pm 52.3)10^6$ M^{-1}. The calorimetric analysis demonstrated that collagen-activated platelets showed significant binding to ranolazine, whereas non-activated platelets showed negligible binding to the compound [Fig. 14]. This finding indicated that ranolazine interacts with the GPVI receptors on platelets induced by collagen. This observation was further confirmed through additional pharmacological assays discussed in the subsequent sections.

Ranolazine attenuated the platelet soluble GPVI level

The post hoc analysis demonstrated that the $FeCl_3$-treated group exhibited statistically significant elevations in the

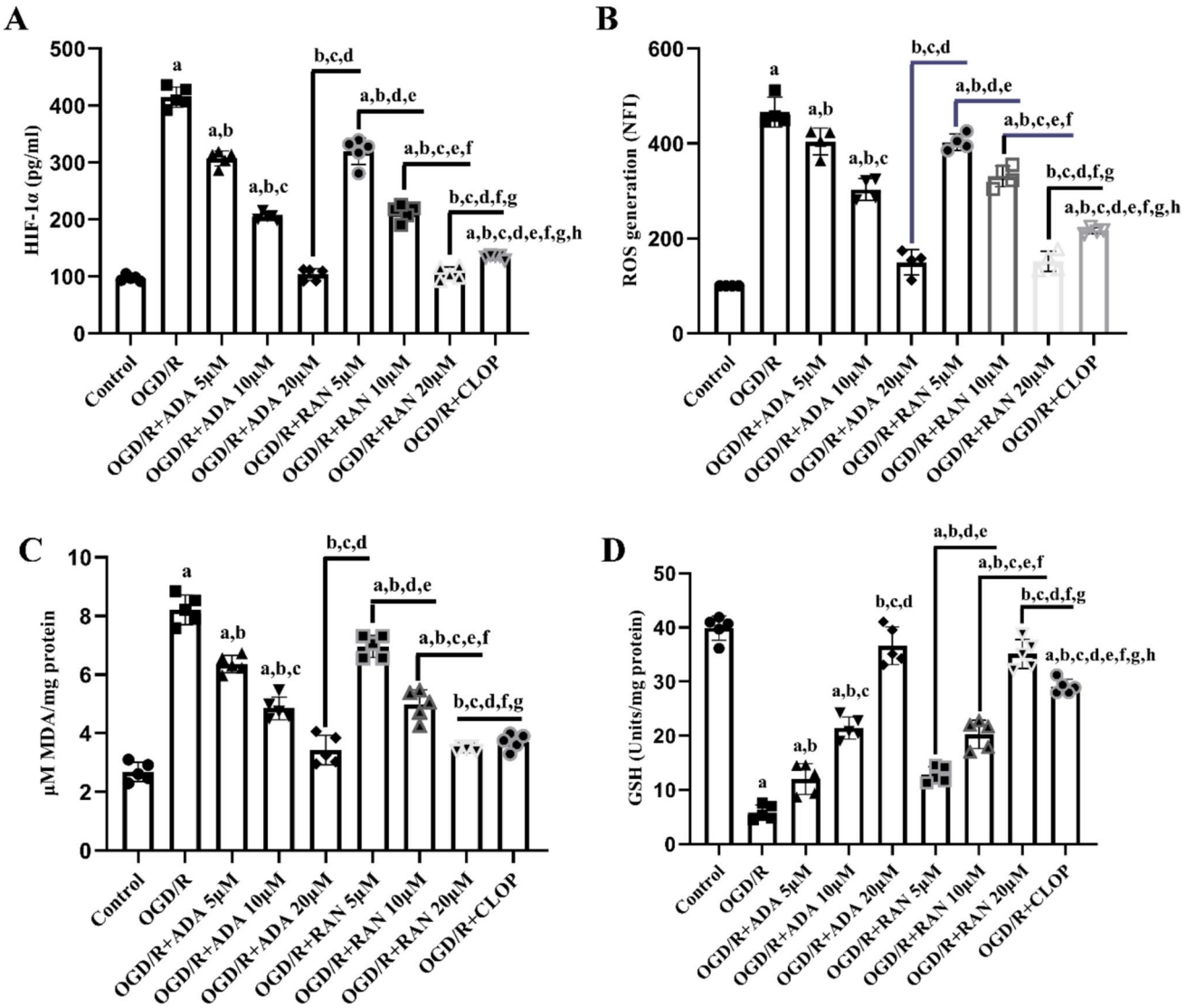

Fig. 11 **A** Adapalene and ranolazine mitigated the HIF-1α level in SHSY5Y cells subjected to OGD/R (n = 5), **B** Adapalene and ranolazine attenuate the ROS level in SHSY5Y cells exposed to OGD/R (n = 4), **C** Adapalene and ranolazine attenuate the MDA level in SHSY5Y cells exposed to OGD/R (n = 5) and **D** adapalene and ranolazine elevated the GSH level in SHSY5Y cells subjected to OGD/R (n = 5). $^{a}p < 0.05$ compared to control, $^{b}p < 0.05$ compared to OGD/R, $^{c}p < 0.05$ compared to OGD/R + 5 µM ADA, $^{d}p < 0.05$ compared to OGD/R + 10 µM ADA, $^{e}p < 0.05$ compared to OGD/R + 20 µM ADA, $^{f}p < 0.05$ compared to OGD/R + 5 µM RAN, $^{g}p < 0.05$ compared to OGD/R + 10 µM RAN, and $^{h}p < 0.05$ compared to OGD/R + 20 µM RAN in their respective groups. All values are represented in the form of mean ± SD. (One-way ANOVA followed by Tukey's multiple comparison post hoc test)

GPVI protein expression compared to the sham-operated rats. Post hoc analysis demonstrated significant variations across the evaluated groups: [F (5, 18) = 63.66; $P < 0.0001$]. Treatment with the 60 mg/kg dose of ranolazine showed a markedly threefold greater decrease in GPVI protein expression compared to the lower 15 mg/kg dose. Losartan was utilized as the standard reference drug, as it is documented to be a GPVI inhibitor (Onselaer et al. 2020). The results of the study did not reveal any statistically significant differences between the $FeCl_3$-exposed groups treated with 15 mg/kg ranolazine and 25 mg/kg losartan [Fig. 15].

Ranolazine attenuates the increased platelet calcium concentrations

The one-way ANOVA demonstrated statistically significant variations across the examined groups: [F (5, 18) = 604.0; $P < 0.0001$]. The post hoc study demonstrated that collagen treatment significantly increased calcium levels. Collagen treatment increased calcium concentration to 61.1 ± 2.46%, while ranolazine 20 µM decreased levels to 13.62 ± 0.86%. The 20 µM ranolazine showed a threefold greater reduction in calcium concentration than 5 µM ranolazine [Fig. 16].

Ranolazine improved platelet cAMP and suppressed plasma COX-1, TXB_2, and PGE_2 levels

The one-way ANOVA test identified statistically significant variances across the groups for the following measures: cAMP [F (5, 24) = 131.1; $P < 0.0001$], COX-1 [F (5, 24) = 98.15; $P < 0.0001$], TXB_2 [F (5, 24) = 94.26; $P < 0.0001$], and PGE_2 [F (5, 24) = 95.59; $P < 0.0001$]. The $FeCl_3$ group showed lower cAMP and higher COX-1, TXB_2, and PGE_2 levels compared to sham-operated controls. Ranolazine treatment in $FeCl_3$ rats increased cAMP and reduced COX-1, TXB_2, and PGE_2 levels compared to untreated $FeCl_3$ rats. However, the 15 mg/kg ranolazine group did not differ significantly in cAMP, COX-1, TXB_2, and PGE_2 levels from the CLOP-treated $FeCl_3$ group [Table 2].

Ranolazine mitigated platelet oxidative stress

The one-way ANOVA indicated significant variations between the experimental groups: ROS [F (5, 24) = 126.2; $P < 0.0001$] [Fig. 17A], H_2O_2 [F (5, 24) = 345.0, $P < 0.0001$] [Fig. 17B], and NOX-1 [F (5, 24) = 101.4: $P < 0.0001$] [Fig. 17C]. $FeCl_3$-treated rats exhibited significantly higher platelet ROS, H_2O_2, and NOX-1 levels compared to sham animals. Ranolazine administration in $FeCl_3$-treated rats attenuated the ROS, H_2O_2, and NOX-1 levels dose-dependently. The 15 mg/kg administration of ranolazine did not demonstrate a significant difference in the levels of platelet ROS, H_2O_2, and NOX-1 when compared to the CLOP-treated $FeCl_3$ group.

Discussion and conclusion

The present study identified adapalene and ranolazine as novel antagonists of the platelet GPVI receptor through a drug repurposing strategy. Extensive in silico and in vitro evaluations confirmed that these repurposed drugs can effectively inhibit platelet aggregation. Moreover, adapalene and ranolazine exhibited neuroprotective effects in an OGD/R cell line model. Subsequent in vivo investigations with ranolazine demonstrated its capacity to influence platelet–ligand interactions, GPVI expression, and calcium levels, alongside biomarkers associated with platelet aggregation and oxidative stress. These results indicate that adapalene and ranolazine possess multifaceted therapeutic capabilities for managing thrombotic and neurological complications, particularly cerebral ischemia.

Initial high-throughput screening pinpointed four compounds: adapalene, ranolazine, azilsartan, and lapatinib, demonstrating superior GPVI binding affinity compared to losartan. Molecular dynamics simulations revealed that adapalene and ranolazine formed strong bonds with and stabilized the GPVI receptor, whereas azilsartan and lapatinib exhibited minimal binding affinities (Supplementary figures S1 and S2). Further, in vitro platelet analysis identified that adapalene and ranolazine effectively inhibited collagen-induced platelet aggregation in a concentration-dependent manner. To confirm the specificity of these antiplatelet actions targeting GPVI, we also assessed the inhibition of platelet aggregation induced by ADP and thrombin. The absence of antiplatelet effects in these latter assays suggests that the selected drugs do not mediate antiplatelet effects through the PAR and P2Y12 receptors, thus indicating that both adapalene and ranolazine exert their antiplatelet effects by inhibiting collagen-mediated platelet aggregation. In addition, flow cytometry was employed to analyze phospho-Syk tyrosine kinase, a recognized marker for GPVI receptor activation following collagen stimulation (Perrella et al. 2022). Our findings demonstrated that treatment with adapalene and ranolazine resulted in a significant reduction in Syk protein expression compared to the collagen group. In alignment with these outcomes, our in vitro studies confirmed that the evaluated compounds diminished collagen-induced platelet aggregation, primarily through the GPVI receptor by impeding Syk phosphorylation. Therefore, we conclude that adapalene and ranolazine effectively inhibit collagen/GPVI-mediated platelet aggregation, positioning them as potential candidates for repurposing as potent GPVI receptor antagonists in the management of thrombotic events (Fig. 18).

Further, in a comparative analysis, adapalene and ranolazine were evaluated against the commercially available drug tirofiban, a known inhibitor of the platelet glycoprotein receptor GPIIb-IIIa (Yang et al. 2019), to assess their efficacy in rapidly inhibiting the platelet aggregation process within a specified period. Our findings demonstrated that both compounds inhibited collagen-mediated platelet activation and aggregation approximately twice as rapidly as the GPIIb–IIIa inhibitor in terms of both platelet activation and aggregation. This suggests that the test compounds demonstrated a rapid inhibitory effect on platelet activation, outperforming the standard compound tirofiban.

Based on the above findings, circular dichroism and Raman spectroscopy were employed to validate computational and experimental findings regarding structural changes in platelets upon incubation with collagen and test compounds. These techniques assessed alterations in platelet structure, particularly the alpha-helical content of proteins like integrin αIIbβ3, which is vital for activation and aggregation (Paul et al. 1999; Yin et al. 2006; Ma et al. 2007). Circular dichroism spectra revealed a significant decrease in alpha-helix content (from 28.52 ± 0.13% to 4.63 ± 0.17%) when platelets were treated with collagen alone compared to those treated with test compounds, indicating altered

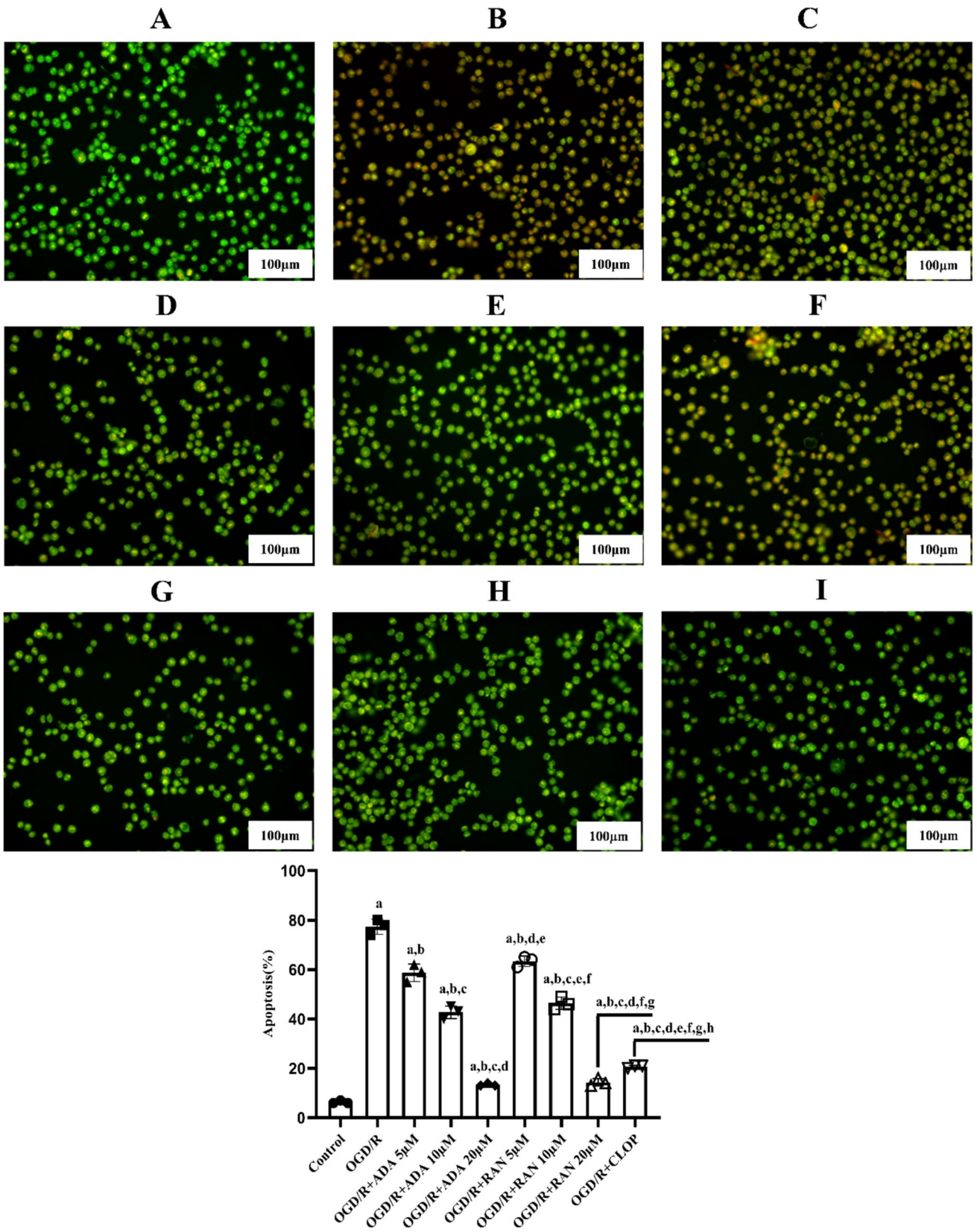
A
B
C
D
E
F
G
H
I
100μm
Apoptosis(%)
0
20
40
60
80
100
a
a,b
a,b,c
a,b,c,d
a,b,d,e
a,b,c,e,f
a,b,c,d,f,g
a,b,c,d,e,f,g,h
Control
OGD/R
OGD/R+ADA 5μM
OGD/R+ADA 10μM
OGD/R+ADA 20μM
OGD/R+RAN 5μM
OGD/R+RAN 10μM
OGD/R+RAN 20μM
OGD/R+CLOP

◂**Fig. 12** Adapalene and ranolazine mitigated apoptosis in the OGD/R-mediated cell death using AO/PI. **A** control, **B** OGD/R, **C** OGD/R + ADA 5 µM, **D** OGD/R + ADA 10 µM, **E** OGD/R + ADA 20 µM, **F** OGD/R + RAN 5 µM, **G** OGD/R + RAN 10 µM, **H** OGD/R + RAN 20 µM, and **I** OGD/R + CLOP 30 µM. [a]$p < 0.05$ compared to control, [b]$p < 0.05$ compared to OGD/R, [c]$p < 0.05$ compared to OGD/R + 5 µM ADA, [d]$p < 0.05$ compared to OGD/R + 10 µM ADA, [e]$p < 0.05$ compared to OGD/R + 20 µM ADA, [f]$p < 0.05$ compared to OGD/R + 5 µM RAN, [g]$p < 0.05$ compared to OGD/R + 10 µM RAN, and.[h]$p < 0.05$ compared to OGD/R + 20 µM RAN in their respective groups. All values are represented in the form of mean ± SD ($n = 3$). (One-way ANOVA followed by Tukey's multiple comparison post hoc test)

conformation. Raman analysis further supported this by showing a shift in the amide I band within the alpha-helix region in collagen-treated platelets. The test compounds were observed to stabilize platelet structure, suggesting they inhibit platelet activation and aggregation by interacting with collagen-binding sites.

Patients on antiplatelet therapy often suffer from bleeding-related adverse effects due to platelet aggregation inhibition (Swan et al. 2020). Our investigation into the test compounds revealed a bleeding risk profile within acceptable limits and superior clotting times compared to clopidogrel, indicating minimal bleeding concerns. Nevertheless, further in vivo studies are necessary to validate potential bleeding-related adverse effects.

After computational and in vitro analyses, we further evaluated the antiplatelet and antithrombotic effects of ranolazine in a rat model of $FeCl_3$-induced carotid artery thrombosis. Initially isothermal titration calorimetry (ITC) experiments assessed the binding affinity of ranolazine to both activated (collagen-stimulated) and resting platelets. Ranolazine demonstrated significant binding affinity for activated platelets, but not for resting platelets, suggesting a specific interaction with collagen-activated platelets and a subsequent inhibition of platelet aggregation. Platelet adhesion to collagen in damaged endothelium occurs via GPVI receptors, initiating platelet aggregation and thrombus formation (Onselaer et al. 2020). Therefore, we quantified GPVI protein expression, a direct marker of platelet activation and aggregation (Pennings et al. 2023). $FeCl_3$ treatment led to increased GPVI protein levels in rats, and ranolazine administration attenuated this elevation in a dose-dependent manner, suggesting that ranolazine functions as an antiplatelet agent by selectively binding to collagen-activated platelets and modulating GPVI expression.

The interaction between collagen and the GPVI receptor on platelets triggers a sustained increase in intracellular calcium (Fernández et al. 2024), initiating a cascade of signaling events that culminate in platelet activation (Tomaiuolo et al. 2017). Consequently, mitigating these calcium levels during platelet activation and aggregation could potentially reduce thrombotic events. Given that ranolazine has been observed to lessen intracellular calcium accumulation in ventricular myocardial cells (Rayner-Hartley and Sedlak 2016), our findings suggest it also effectively reduces increased intracellular calcium levels in platelets activated by collagen. This suggests ranolazine's potent capacity to decrease calcium concentrations, potentially offering significant benefits in managing platelet aggregation and thrombosis associated with ischemic stroke.

Further, activation of GPVI and elevated intracellular calcium in platelets trigger thromboxane (Greer 1987) and prostaglandin E_2 production via cyclooxygenase 1, leading to platelet activation, aggregation (MacIntyre and Gordon 1975; Sakata et al. 2013), and reduced cAMP levels (Noe et al. 2010). Ranolazine has been shown to enhance cAMP in endothelial cell culture (Fu et al. 2013). Our study found that $FeCl_3$ treatment decreased platelet cAMP and increased plasma levels of COX-1, TXB_2, and PGE_2, indicating platelet activation. Conversely, ranolazine treatment in $FeCl_3$-induced rats increased cAMP and decreased COX-1, TXB_2, and PGE_2, suggesting that ranolazine inhibits platelet activation and aggregation by interfering with multiple agonists, thereby preventing clot formation. Further research is needed to determine if ranolazine independently modulates these mediators, as these are also regulated by other platelet agonists.

Platelet activation, particularly via GPVI, generates ROS (Ghasemzadeh and Hosseini 2017), further amplifying activation. Previous studies indicated ranolazine's antioxidant effects in C2C12 skeletal muscle cells (Ileana et al. 2017). Our findings show that ranolazine treatment reduced ROS, hydrogen peroxide, and NOX-1 (a crucial enzyme responsible for ROS generation (Carrim et al. 2015)) levels, suggesting that ranolazine has free radical scavenging properties that may contribute to its anti-aggregation effects. Although adapalene demonstrated potent antiplatelet activity in vitro, but was not evaluated in an in vivo $FeCl_3$ model due to its poor pharmacokinetic properties, including low solubility and bioavailability (Aura et al. 2020), and its inability to cross the blood–brain barrier (Medina et al. 2019, 2020). Future research should evaluate its in vivo antiplatelet efficacy using novel formulations. Ranolazine was selected for in vivo studies based on prior research highlighting its favorable systemic bioavailability and pharmacokinetic profile (Mashayekhi-Sardoo et al. 2022), available toxicity data (Rayner-Hartley and Sedlak 2016), absence of bleeding risk (Reddy et al. 2010; Codolosa et al. 2014; Meenakshisundaram et al. 2015), documented neuroprotective effects in clinical studies (Akgul et al. 2024), and capacity to cross the blood–brain barrier (Kahlig et al. 2010).

Following platelet activation and aggregation, clot formation occurs, a key feature of ischemic stroke. To manage this, the FDA has approved antiplatelet agents for both primary treatment and secondary stroke prevention. In addition,

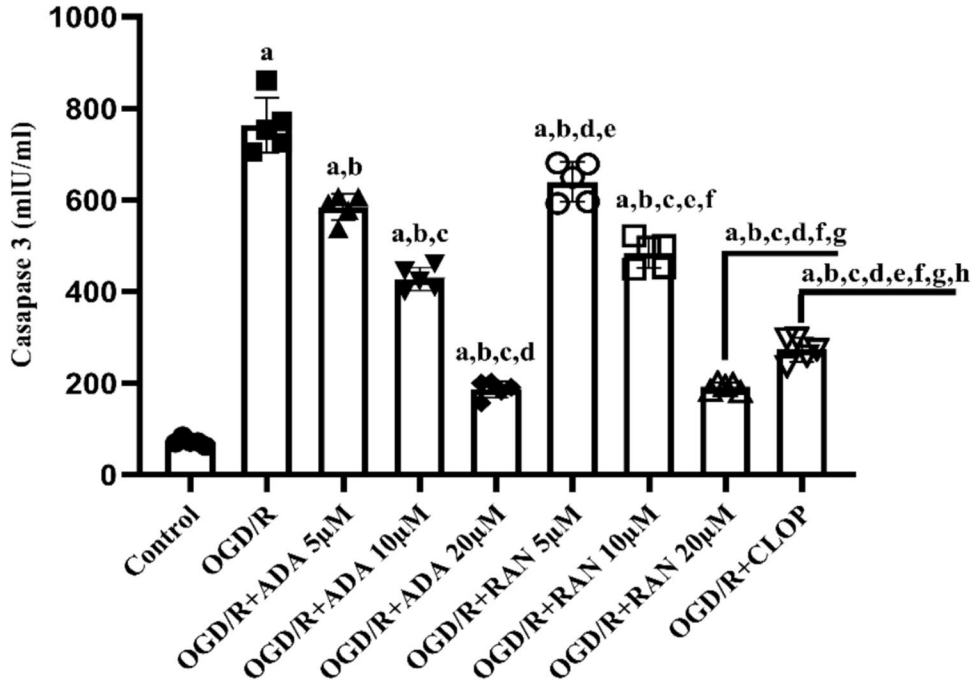

Fig. 13 Adapalene and ranolazine attenuated the caspase-3 level in the OGD/R-mediated cell apoptosis. **A** control, **B** OGD/R, **C** OGD/R + ADA 5 μM, **D** OGD/R + ADA 10 μM, **E** OGD/R + ADA 20 μM, **F** OGD/R + RAN 5 μM, **G** OGD/R + RAN 10 μM, **H** OGD/R + RAN 20 μM, and **I** OGD/R + CLOP 30 μM. [a]$p < 0.05$ compared to control, [b]$p < 0.05$ compared to OGD/R, [c]$p < 0.05$ compared to OGD/R + 5 μM ADA, [d]$p < 0.05$ compared to OGD/R + 10 μM ADA, [e]$p < 0.05$ compared to OGD/R + 20 μM ADA, [f]$p < 0.05$ compared to OGD/R + 5 μM RAN, [g]$p < 0.05$ compared to OGD/R + 10 μM RAN, and [h]$p < 0.05$ compared to OGD/R + 20 μM RAN in their respective groups. All values are represented in the form of mean ± SD ($n = 5$). (One-way ANOVA followed by Tukey's multiple comparison post hoc test)

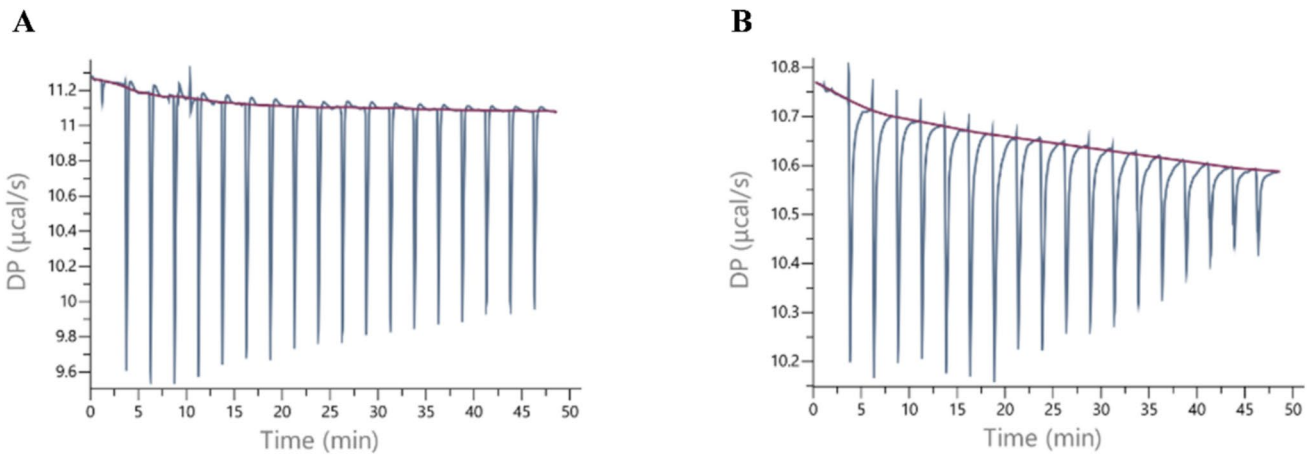

Fig. 14 A representative titration curve **A** shows that ranolazine does not interact with resting platelets, while **B** demonstrates the interaction of ranolazine with collagen-activated platelets, as measured by isothermal titration calorimetry ($n = 3$)

neuroprotective medications are employed in stroke management to shield ischemic brain neurons from irreversible damage and prevent neuronal degeneration (Sharma 2016; Rai et al. 2024), a strategy recommended by the Stroke Therapy Academic Industry Roundtable (STAIR) to reduce brain infarction (Ramakrishna et al. 2022b). Adapalene and ranolazine have been identified as potential GPVI receptor antagonists, suggesting their application as antiplatelet agents in the treatment and management of thrombotic disorders, like ischemic stroke. Indeed, adapalene is used in clinics to manage the various dermatological conditions, including acne vulgaris (Rusu et al. 2020), and ranolazine

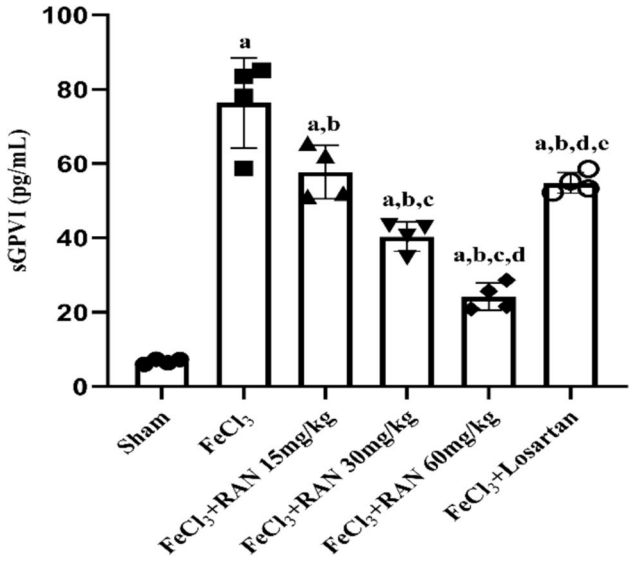

Fig. 15 Ranolazine mitigated platelet sGPVI level. $^{a}p<0.05$ compared to sham, $^{b}p<0.05$ compared to $FeCl_3$, $^{c}p<0.05$ compared to $FeCl_3+15$ mg/kg RAN, $^{d}p<0.05$ compared to $FeCl_3+30$ mg/kg RAN, and $^{e}p<0.05$ compared to $FeCl_3+60$ mg/kg RAN in their respective groups. All values are represented in the form of mean ± SD ($n=4$). (One-way ANOVA followed by Tukey's multiple comparison post hoc test)

is prescribed for chronic angina (Aldakkak et al. 2013). Ranolazine has also been documented to possess neuroprotective effects against conditions such as Alzheimer's disease (Samir et al. 2024), neuroinflammation (Cassano et al. 2022), and dementia (Samir et al. 2024), indicating its potential as a neuroprotective agent. However, the neuroprotective effects of adapalene have not yet been investigated. Therefore, considering the importance of their antiplatelet activities for treating and managing ischemic stroke, we postulate that these drugs could also function as neuroprotective agents in combating cerebral ischemia. To prove it, we assessed their neuroprotective capabilities in SHSY5Y cell lines, utilizing an oxygen–glucose deprivation/reperfusion (OGD/R) induced neuronal injury model that replicates the cellular damage occurring post-stroke.

Correspondingly, adapalene and ranolazine conferred neuroprotection, as evidenced by augmented cell viability in OGD/R-exposed cells. OGD/R injury triggers the mitochondrial permeability transition pore, consequently diminishing the mitochondrial membrane potential (Su et al. 2021), a crucial determinant of cellular viability, ultimately culminating in cellular bioenergetic failure and subsequent apoptosis (Hendgen-Cotta et al. 2019; Rai 2021). Our results demonstrate that OGD/R insult precipitated a marked reduction in MMP, which was more robustly restored by adapalene and ranolazine, indicating that both compounds ameliorated the viability of SHSY5Y cells subjected to OGD/R, potentially through the enhancement of MMP. Further assessments were conducted on the levels of various ischemic markers within SHSY5Y cells to prove the neuroprotective activity of test drugs in the cerebral ischemic model. Notably, HIF-1α, a crucial transcriptional regulator induced by hypoxic conditions and implicated in apoptotic cell death (Wei et al. 2022; Prajapati et al. 2025), was observed to be elevated following OGD/R, with both adapalene and ranolazine demonstrating a reversal of this effect. OGD/R injury induces oxidative stress, diminishing antioxidant enzyme (GSH) activity while concurrently increasing oxidative stress markers such as ROS and MDA (Dharmajaya and Sari 2022; Jomova et al. 2023; Yu et al. 2024; Ramakrishna et al. 2025). The elevation in HIF-1α levels has also been positively linked to increased ROS during hypoxia (Qutub and Popel 2008). Treatment with both adapalene and ranolazine led to a significant reduction in ROS and MDA levels and an improvement in GSH levels in SHSY5Y cells, suggesting an antioxidant role for both compounds in mitigating cellular stress. Furthermore, the accumulation of ROS under oxidative stress contributes to cell death (Wu et al. 2020a; Singh et al. 2024); therefore, apoptosis was evaluated using acridine orange and propidium iodide staining, alongside caspase-3 level measurements. These assessments confirmed that both drugs reduced apoptosis, as evidenced by the staining methods, and decreased caspase-3 levels. In summary, our in vitro neuroprotection studies indicate that adapalene and ranolazine confer significant neuroprotection against OGD/R injury in neuronal cell lines by ameliorating HIF-1α, mitochondrial dysfunction, oxidative stress, and apoptosis.

Adapalene and ranolazine, at higher doses, demonstrated a notable capacity to restore cell viability, exceeding 80.00%. Clopidogrel also contributed to improved viability (72.22%), albeit to a lesser extent. This suggests that adapalene and ranolazine possess superior neuroprotective potential against ischemic neuronal injury compared to clopidogrel. While clopidogrel is recognized for its antiplatelet role in treating ischemic stroke, it is not recommended for neuroprotection. Interestingly, adapalene and ranolazine exhibited comparable antiplatelet effects without increasing bleeding time, and provided enhanced neuroprotection over clopidogrel, indicating their suitability for effective ischemic stroke management. These results underscore the superior neuroprotective properties of both adapalene and ranolazine relative to clopidogrel, identifying them as potential candidates for advanced preclinical and clinical development in cerebral stroke therapy. Further research is necessary to determine if neuroprotection is achieved through platelet inhibition or other mechanisms.

In conclusion, this study systematically investigated the antiplatelet and neuroprotective properties of adapalene and ranolazine via a drug repurposing strategy. Both compounds demonstrated significant antiplatelet and neuroprotective activities, evidenced by the mitigation of platelet

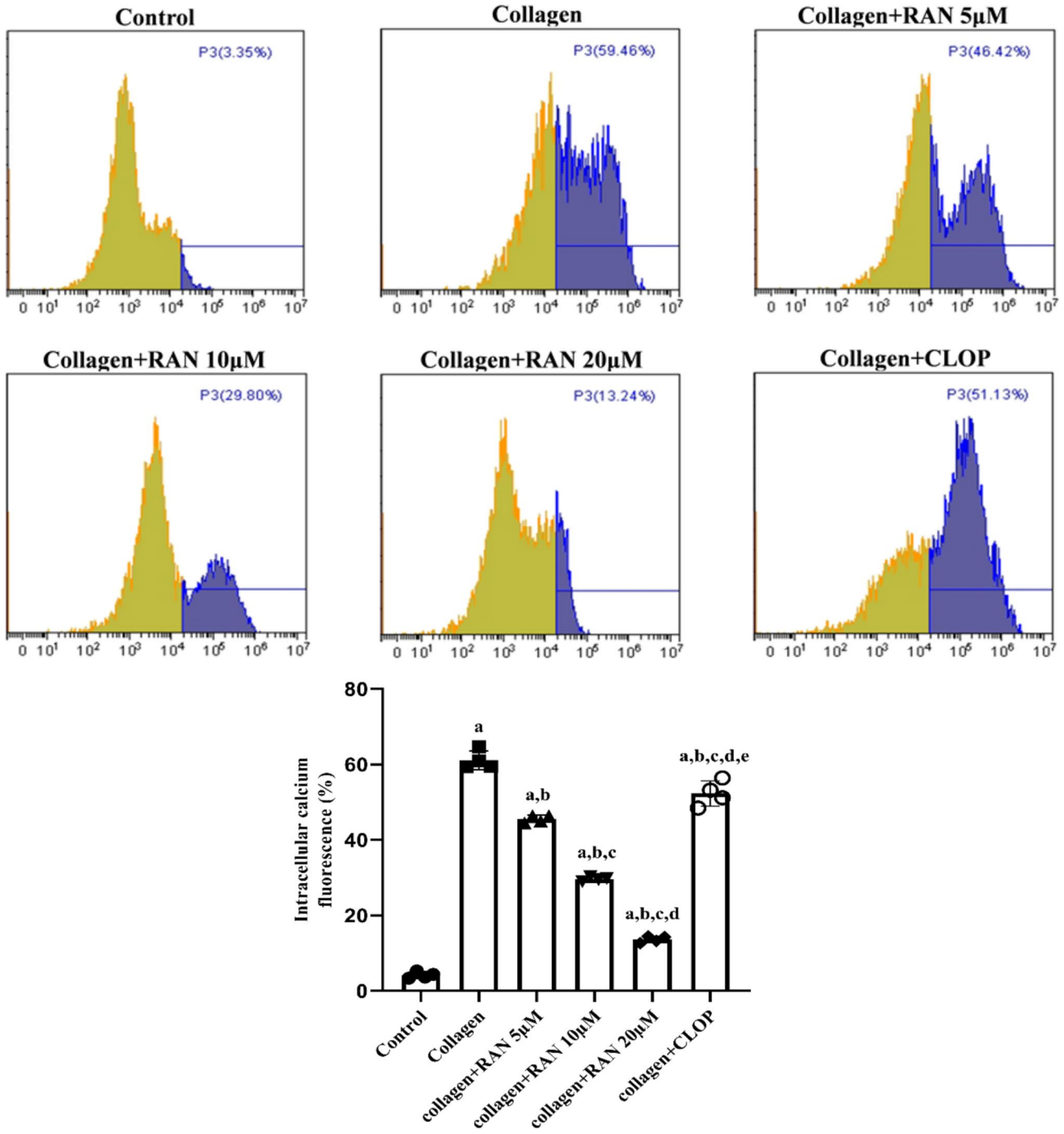

Fig. 16 Ranolazine attenuated platelet calcium level using Fura-2AM analyzed via flow cytometry. [a]$p < 0.05$ compared to control, [b]$p < 0.05$ compared to collagen, [c]$p < 0.05$ compared to collagen + 5 μM RAN, [d]$p < 0.05$ compared to collagen + 10 μM RAN, and [e]$p < 0.05$ compared to collagen + 20 μM RAN in their respective groups. All values are represented in the form of mean ± SD ($n = 4$). (One-way ANOVA followed by Tukey's multiple comparison post hoc test)

aggregation, aggregation markers, oxidative stress, hypoxic stress, mitochondrial dysfunction, and apoptosis. Furthermore, their combined antiplatelet and neuroprotective capacities suggest potential multifaceted therapeutic benefits for managing both primary and secondary strokes, as well as post-stroke neuronal injury. Subsequent research should prioritize the validation of these in vitro findings using in vivo models to enhance translational applicability. This includes acknowledging the inherent limitations of rodent models in fully recapitulating human physiological responses,

Table 2 Ranolazine (15, 30, and 60 mg/kg) decreases the COX-1, PGE_2, and TXB_2 levels while increasing the cAMP levels in a $FeCl_3$ model. [a]$p < 0.05$ compared to sham, [b]$p < 0.05$ compared to $FeCl_3$, [c]$p < 0.05$ compared to $FeCl_3 + 15$ mg/kg RAN, [d]$p < 0.05$ compared to $FeCl_3 + 30$ mg/kg RAN, and [e]$p < 0.05$ compared to $FeCl_3 + 60$ mg/kg RAN in their respective groups

Markers (pg/ml)	Sham	$FeCl_3$	$FeCl_3$ + RAN 15 mg/kg	$FeCl_3$ + RAN 30 mg/kg	$FeCl_3$ + RAN 60 mg/kg	$FeCl_3$ + CLOP 40 mg/kg
cAMP	80.67 ± 4.28	33.25 ± 3.64[a]	47.1 ± 1.97[a,b]	58.05 ± 3.34[a,b,c]	72.15 ± 3.13[a,b,c,d]	51.19 ± 3.38[a,b,d,e]
COX-1	44.93 ± 4.08	155.52 ± 13.5[a]	116.86 ± 1.95[a,b]	84.1 ± 12.16[a,b,c]	63.01 ± 8.05[a,b,c,d]	115.35 ± 6.86[a,b,d,e]
PGE_2	26.59 ± 3.85	150.21 ± 9.57[a]	100.68 ± 12.25[a,b]	72.05 ± 8.15[a,b,c]	46.81 ± 11.12[a,b,c,d]	100.95 ± 12.88[a,b,d,e]
TXB_2	424.76 ± 14.35	736.29 ± 43.96[a]	670.62 ± 10.07[a,b]	572.98 ± 25.71[a,b,c]	485.36 ± 23.63[a,b,c,d]	628.11 ± 29.27[a,b,d,e]

All values are represented in the form of mean ± SD ($n = 5$). (One-way ANOVA followed by Tukey's multiple comparison post hoc test).

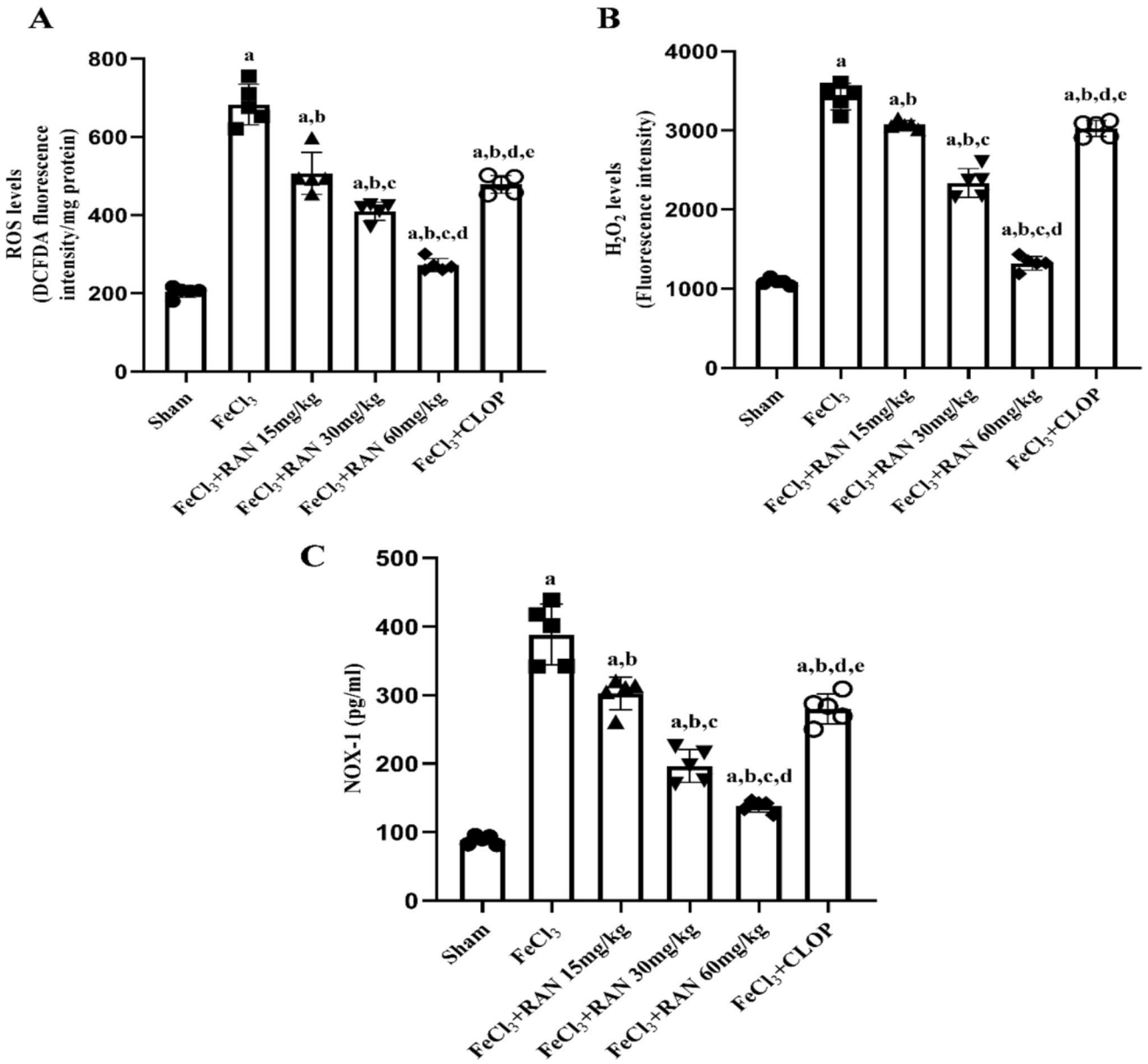

Fig. 17 Ranolazine alleviated the platelets ROS (**A**), H_2O_2 (**B**), and NOX-1 (**C**) levels after $FeCl_3$-induced carotid artery thrombosis model. [a]$p < 0.05$ compared to sham, [b]$p < 0.05$ compared to $FeCl_3$, [c]$p < 0.05$ compared to $FeCl_3 + 15$ mg/kg RAN, [d]$p < 0.05$ compared to $FeCl_3 + 30$ mg/kg RAN, and [e]$p < 0.05$ compared to $FeCl_3 + 60$ mg/kg RAN in their respective groups. All values are represented in the form of mean ± SD ($n = 5$). (One-way ANOVA followed by Tukey's multiple comparison post hoc test).

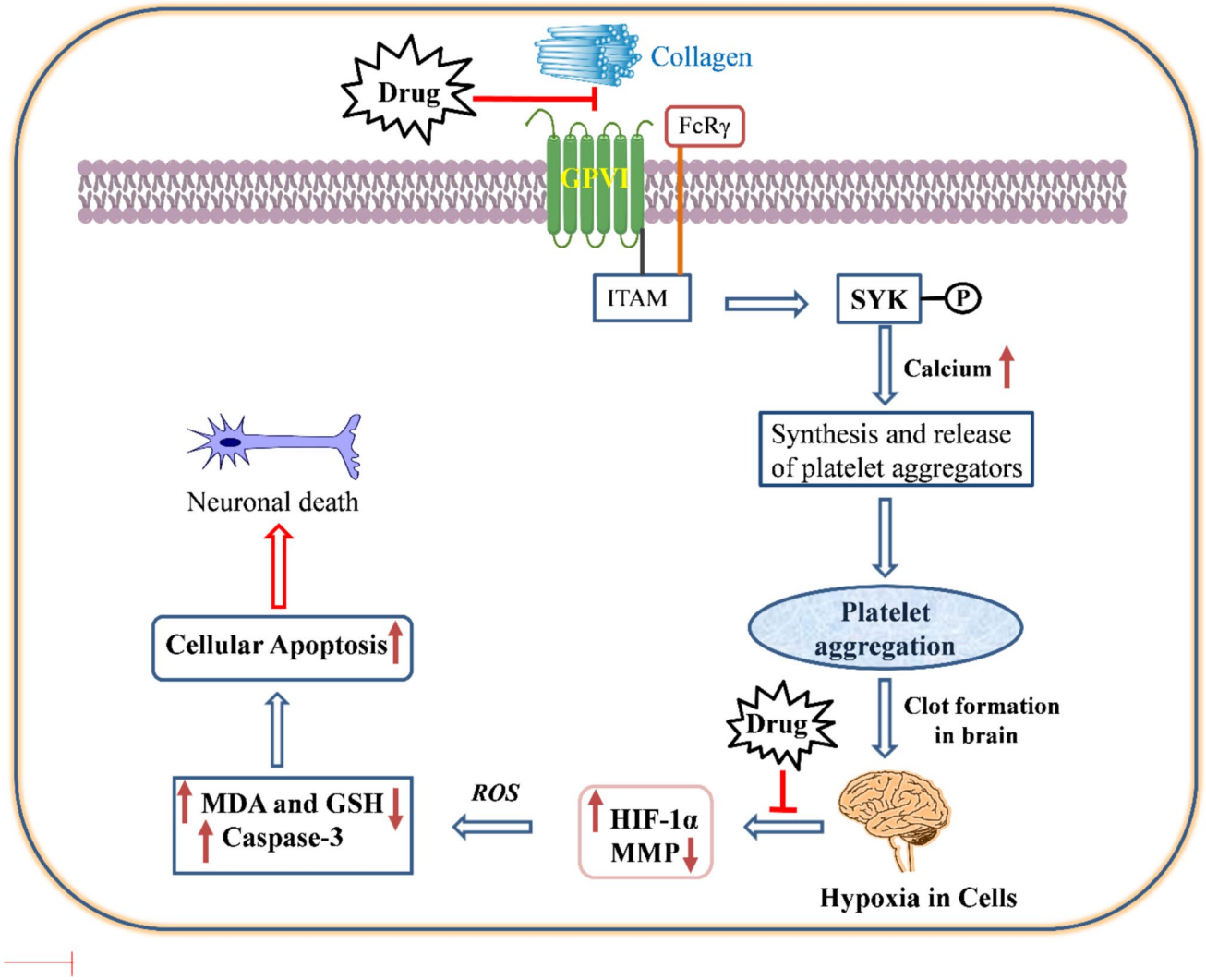

Fig. 18 Antiplatelet and neuroprotective mechanisms of adapalene and ranolazine (inhibition – '⊣')

particularly concerning drug metabolism and systemic interactions. Ultimately, prospective clinical trials are imperative to ascertain the efficacy of adapalene and ranolazine as GPVI inhibitors and for neuroprotection against cerebral ischemia.

Supplementary Information The online version contains supplementary material available at https://doi.org/10.1007/s13205-025-04530-z.

Acknowledgements The authors express gratitude to IIT-BHU and CDC-BHU, Varanasi, for providing access to flow cytometry and fluorescence imaging resources. M.A.S acknowledges the financial support received from the Ministry of Education, India, for research endeavors.

Author contributions Mohammad.A.S. was responsible for conceptualization; methodology; in silico, in vitro, and in vivo studies; investigation; and writing of the original draft, review, and editing. Poorvi S. and S.K.S. helped in computational studies, investigations, reviews, and editing. Sudha M. P. and Debabrata M. helped in in vitro studies. Ravi S. helped in computational studies. Abhishek P. helped in in vivo studies. Kakarla reviewed and edited the manuscript. Sairam.K. helped with the experimental design, supervision, conceptualization, reviewing, and editing of the manuscript.

Data availability Data will be made available on request.

Declarations

Conflict of interest The authors report no known competing financial interests or personal relationships that may have influenced the work described in this paper.

Ethical approval All experimental procedures were carried out in accordance with the guidelines established by the Committee for the Purpose of Control and Supervision of Experiments on Animals, India, as well as the regulations outlined in the National Institutes of Health Guide for Laboratory Animal Care and Use. Prior to the initiation of the study, approval was obtained from the Institutional Animal Ethics Committee, assigned the approval number IIT(BHU)/IAEC/2023/027.

References

Akgul E, Gunduz MK, Parlar Aİ, Guner Y, Eroglu M, Ozhan A, Alptekin GS, Cekirdekci A (2024) The anti-apoptotic effect of ranolazine on cerebral protection during cardiopulmonary bypass and carotid artery surgery. Acta Cardiol Sin 40(1):77

Aldakkak M, Stowe DF, Camara AK (2013) Safety and efficacy of ranolazine for the treatment of chronic angina pectoris. Clin Med Insights: Therapeut 5:CMT-S7824

Aura R, Corneliu T, Georgiana AP, Nicoleta T (2020) Recent advances regarding the the rapeutic potential of adapalene. Pharmaceuticals 13(9):217. https://doi.org/10.3390/ph13090217

Alluri H, Shaji CA, Davis ML, Tharakan B (2015) Oxygen-glucose deprivation and reoxygenation as an in vitro ischemia-reperfusion injury model for studying blood-brain barrier dysfunction. JoVE (Journal of Visualized Experiments) 99:e52699

Al-Tamimi M, Tan CW, Qiao J, Pennings GJ, Javadzadegan A, Yong AS, Arthur JF, Davis AK, Jing J, Mu F-T (2012) Pathologic shear triggers shedding of vascular receptors: a novel mechanism for down-regulation of platelet glycoprotein VI in stenosed coronary vessels. Blood J Am Soc Hematol 119(18):4311–4320

Amar SK, Donohue KB, Gust KA (2023) Cellular and molecular responses to ethyl-parathion in undifferentiated SH-SY5Y cells provide neurotoxicity pathway indicators for organophosphorus impacts. Toxicol Sci 191(2):285–295

Arora M, Ganugula R, Kumar N, Kaur G, Pellois J-P, Garg P, Ravi Kumar M (2019) Next-generation noncompetitive nanosystems based on gambogic acid: in silico identification of transferrin receptor binding sites, regulatory shelf stability, and their preliminary safety in healthy rodents. ACS Appl Bio Mater 2(8):3540–3550

Asada Y, Yamashita A, Sato Y, Hatakeyama K (2018) Thrombus formation and propagation in the onset of cardiovascular events. J Atheroscler Thromb 25(8):653–664

Assumpção TC, Alvarenga PH, Ribeiro JM, Andersen JF, Francischetti IM (2010) Dipetalodipin, a novel multifunctional salivary lipocalin that inhibits platelet aggregation, vasoconstriction, and angiogenesis through unique binding specificity for TXA2, PGF2α, and 15 (S)-HETE. J Biol Chem 285(50):39001–39012

Beck S, Öftering P, Li R, Hemmen K, Nagy M, Wang Y, Zarpellon A, Schuhmann MK, Stoll G, Ruggeri ZM (2023) Platelet glycoprotein V spatio-temporally controls fibrin formation. Nat Cardiovasc Res 2(4):368–382

Benjamin EJ, Virani SS, Callaway CW, Chamberlain AM, Chang AR, Cheng S, Chiuve SE, Cushman M, Delling FN, Deo R (2018) Heart disease and stroke statistics—2018 update: a report from the American Heart Association. Circulation 137(12):e67–e492

Carrim N, Arthur JF, Hamilton JR, Gardiner EE, Andrews RK, Moran N, Berndt MC, Metharom P (2015) Thrombin-induced reactive oxygen species generation in platelets: A novel role for protease-activated receptor 4 and GPIbα. Redox Biol 6:640–647

Cassano V, Tallarico M, Armentaro G, De Sarro C, Iannone M, Leo A, Citraro R, Russo E, De Sarro G, Hribal ML (2022) Ranolazine attenuates brain inflammation in a rat model of type 2 diabetes. Int J Mol Sci 23(24):16160

Chapman SN, Mehndiratta P, Johansen MC, McMurry TL, Johnston KC, Southerland AM (2014) Current perspectives on the use of intravenous recombinant tissue plasminogen activator (tPA) for treatment of acute ischemic stroke. Vasc Health Risk Manag. https://doi.org/10.2147/VHRM.S39213

Cheng T-F, Zhao J, Wu Q-L, Zeng H-W, Sun Y-T, Zhang Y-H, Mi R, Qi X-P, Zou J-T, Liu A-J (2020) Compound dan zhi tablet attenuates experimental ischemic stroke via inhibiting platelet activation and thrombus formation. Phytomedicine 79:153330

Ciborowski M, Tomasiak M (2009) The *in vitro* effect of eptifibatide, a glycoprotein IIb/IIIa antagonist, on various responses of porcine blood platelets. Acta Pol Pharm 66(3):235–242

Codolosa JN, Acharjee S, Figueredo VM (2014) Update on ranolazine in the management of angina. Vasc Health Risk Manag. https://doi.org/10.2147/VHRM.S40477

Dharmajaya R, Sari DK (2022) Malondialdehyde value as radical oxidative marker and endogenous antioxidant value analysis in brain tumor. Ann Med Surg. https://doi.org/10.1016/j.amsu.2021.103231

Duffett L (2022) Deep venous thrombosis. Ann Intern Med 175(9):ITC129–ITC144

Feitsma LJ, Brondijk HC, Jarvis GE, Hagemans D, Bihan D, Jerah N, Versteeg M, Farndale RW, Huizinga EG (2022) Structural insights into collagen binding by platelet receptor glycoprotein VI. Blood, J Am Soc Hematol 139(20):3087–3098

Feldman A, Sun D, Law M, Novak A, Attygalle A, Thorland E, Fink S, Vrana J, Caron B, Morice W (2008) Overexpression of Syk tyrosine kinase in peripheral T-cell lymphomas. Leukemia 22(6):1139–1143

Fernández DI, Troitiño S, Sobota V, Tullemans BM, Zou J, van den Hurk H, García Á, Honarnejad S, Kuijpers MJ, Heemskerk JW (2024) Ultra-high throughput-based screening for the discovery of antiplatelet drugs affecting receptor dependent calcium signaling dynamics. Sci Rep 14(1):6229

Fu Z, Zhao L, Chai W, Dong Z, Cao W, Liu Z (2013) Ranolazine recruits muscle microvasculature and enhances insulin action in rats. J Physiol 591(20):5235–5249

Genheden S, Ryde U (2015) The MM/PBSA and MM/GBSA methods to estimate ligand-binding affinities. Expert Opin Drug Discov 10(5):449–461

Gervin E, Shin B, Opperman R, Cullen M, Feser R, Maiti S, Majumder M (2020) Chemically induced hypoxia enhances miRNA functions in breast cancer. Cancers 12(8):2008

Ghasemzadeh M, Hosseini E (2017) Platelet granule release is associated with reactive oxygen species generation during platelet storage: a direct link between platelet pro-inflammatory and oxidation states. Thromb Res 156:101–104

Gillespie S, Holloway PM, Becker F, Rauzi F, Vital SA, Taylor KA, Stokes KY, Emerson M, Gavins FN (2018) The isothiocyanate sulforaphane modulates platelet function and protects against cerebral thrombotic dysfunction. Br J Pharmacol 175(16):3333–3346

Greer I (1987) Therapeutic progress–review XXVIII: platelet function and calcium channel blocking agents. J Clin Pharm Ther 12(4):213–222

Gresele P, Momi S (2022a) Novel approaches to antiplatelet therapy. Biochem Pharmacol. https://doi.org/10.1016/j.bcp.2022.115297

Gresele P, Momi S (2022b) Novel approaches to antiplatelet therapy. Biochem Pharmacol 206:115297

Harper MT, Van Den Bosch MT, Hers I, Poole AW (2013) Absence of platelet phenotype in mice lacking the motor protein myosin Va. PLoS ONE 8(1):e53239

Hendgen-Cotta UB, Giorgio V, Hool L (2019) Mitochondria at the crossroads of survival and demise. Oxid Med Cell Longev. https://doi.org/10.1155/2019/2608187

Horii K, Kahn ML, Herr AB (2006) Structural basis for platelet collagen responses by the immune-type receptor glycoprotein VI. Blood 108(3):936–942

Huang Y, Wang Z, Huang Z-X, Liu Z (2023) Biomarkers and the outcomes of ischemic stroke. Front Mol Neurosci 16:1171101

Ileana T, Anna M, Pamela S, Fernanda V, Stefano B, Livio L (2017) Ranolazine promotes muscle differentiation and reduces oxidative stress in C2C12 skeletal muscle cells. Endocrine 58:33–45

Jiang P, Loyau S, Tchitchinadze M, Ropers J, Jondeau G, Jandrot-Perrus M (2015) Inhibition of glycoprotein VI clustering by

collagen as a mechanism of inhibiting collagen-induced platelet responses: the example of losartan. PLoS ONE 10(6):e0128744
Jomova K, Raptova R, Alomar SY, Alwasel SH, Nepovimova E, Kuca K, Valko M (2023) Reactive oxygen species, toxicity, oxidative stress, and antioxidants: chronic diseases and aging. Arch Toxicol 97(10):2499–2574
Jourdi G, Lordkipanidze M, Philippe A, Bachelot-Loza C, Gaussem P (2021) Current and novel antiplatelet therapies for the treatment of cardiovascular diseases. Int J Mol Sci 22(23):13079
Juntunen M, Hagman S, Moisan A, Narkilahti S, Miettinen S (2020) (2020) In vitro oxygen-glucose deprivation-induced stroke models with human neuroblastoma cell-and induced pluripotent stem cell-derived neurons. Stem Cells Int 1:884126
Kahlig KM, Lepist I, Leung K, Rajamani S, George AL (2010) Ranolazine selectively blocks persistent current evoked by epilepsy-associated NaV1. 1 mutations. Br J Pharmacol 161(6):1414–1426
Kamarova M, Baig S, Patel H, Monks K, Wasay M, Ali A, Redgrave J, Majid A, Bell SM (2022) Antiplatelet use in ischemic stroke. Ann Pharmacother 56(10):1159–1173
Kashyap D, Varshney N, Baral B, Kandpal M, Indari O, Jain AK, Chatterji D, Kumar S, Parmar HS, Sonawane A (2023) *Helicobacter pylori* infected gastric epithelial cells bypass cell death pathway through the oncoprotein Gankyrin. Adv Cancer Biol-Metastasis 7:100087
Kharazian B, Lohse SE, Ghasemi F, Raoufi M, Saei AA, Hashemi F, Farvadi F, Alimohamadi R, Jalali SA, Shokrgozar MA (2018) Bare surface of gold nanoparticle induces inflammation through unfolding of plasma fibrinogen. Sci Rep 8(1):12557
Kumar N, Gahlawat A, Kumar RN, Singh YP, Modi G, Garg P (2022) Drug repurposing for Alzheimer's disease: in silico and in vitro investigation of FDA-approved drugs as acetylcholinesterase inhibitors. J Biomol Struct Dyn 40(7):2878–2892
Kundalevich A, Kapitunova A, Berezin K, Zyubin A, Moiseeva E, Rafalskiy V, Samusev I (2024) Raman spectra simulation of antiplatelet drug-platelet interaction using DFT. Sci Rep 14(1):1445
Li RH, Nguyen N, Rosati T, Jandrey K (2020) Assessment of P2Y12 inhibition by clopidogrel in feline platelets using flow cytometry quantification of vasodilator-stimulated phosphoprotein phosphorylation. Front Vet Sci 7:267
Lin K, Zhang Z, Zhang Z, Zhu P, Jiang X, Wang Y, Deng Q, Lam Yung KK, Zhang S (2021) Oleanolic acid alleviates cerebral ischemia/reperfusion injury via regulation of the GSK-3β/HO-1 signaling pathway. Pharmaceuticals 15(1):1
Liu H-Y, Du L, Zhao Y-T, Tian W-Q (2015) In vitro hemocompatibility and cytotoxicity evaluation of halloysite nanotubes for biomedical application. J Nanomater 2015(1):685323
Liu C, Guo H, DaSilva NA, Li D, Zhang K, Wan Y, Gao X-H, Chen H-D, Seeram NP, Ma H (2019) Pomegranate (*Punica granatum*) phenolics ameliorate hydrogen peroxide-induced oxidative stress and cytotoxicity in human keratinocytes. J Funct Foods 54:559–567
Ma YQ, Qin J, Plow E (2007) Platelet integrin αIIbβ3: activation mechanisms. J Thromb Haemost 5(7):1345–1352
MacIntyre D, Gordon J (1975) Calcium-dependent stimulation of platelet aggregation by PGE2. Nature 258(5533):337–339
Makhoul S, Dorschel S, Gambaryan S, Walter U, Jurk K (2019a) Feedback regulation of Syk by protein kinase C in human platelets. Int J Mol Sci 21(1):176
Makhoul S, Trabold K, Gambaryan S, Tenzer S, Pillitteri D, Walter U, Jurk K (2019b) cAMP-and cGMP-elevating agents inhibit GPIbα-mediated aggregation but not GPIbα-stimulated Syk activation in human platelets. Cell Commun Signal 17:1–20
Marchelak A, Kolodziejczyk-Czepas J, Ponczek MB, Liudvytska O, Markowicz-Piasecka M, Bielska B, Miłowska K, Olszewska MA (2023) Flavonol and A-type procyanidin-rich extracts of *Prunus spinosa* L. flower exhibit anticoagulant activity through direct thrombin inhibition, but do not affect platelet aggregation *in vitro*. Front Pharmacol 14:1307373
Mashayekhi-Sardoo H, Kamali H, Mehri S, Sahebkar A, Imenshahidi M, Mohammadpour AH (2022) Comparison of pharmacokinetic parameters of ranolazine between diabetic and non-diabetic rats. Iran J Basic Med Sci 25(7):865
Medina DX, Chung EP, Bowser R, Sirianni RW (2019) Lipid and polymer blended polyester nanoparticles loaded with adapalene for activation of retinoid signaling in the CNS following intravenous administration. J Drug Deliv Sci Technol 52:927–933
Medina DX, Chung EP, Teague CD, Bowser R, Sirianni RW (2020) Intravenously administered, retinoid activating nanoparticles increase lifespan and reduce neurodegeneration in the SOD1G93A mouse model of ALS. Front Bioeng Biotechnol 8:224
Meenakshisundaram R, Cannie DE, Shankar PR, Zadeh HZ, Bajracharya O, Thirumalaikolundusubramanian P (2015) Cardiovascular Toxicity of Cardiovascular Drugs. In: Heart and Toxins. Elsevier, pp 225–274
Murad JP, Espinosa EV, Ting HJ, Khasawneh FT (2012) Characterization of the in vivo antiplatelet activity of the antihypertensive agent losartan. J Cardiovasc Pharmacol Ther 17(3):308–314
Nazıroğlu M, Çiğ B, Yazğan Y, Schwaerzer GK, Theilig F, Pecze L (2019) Albumin evokes Ca2+-induced cell oxidative stress and apoptosis through TRPM2 channel in renal collecting duct cells reduced by curcumin. Sci Rep 9(1):12403
Noe L, Peeters K, Izzi B, Van Geet C, Freson K (2010) Regulators of platelet cAMP levels: clinical and therapeutic implications. Curr Med Chem 17(26):2897–2905
Onselaer M-B, Nagy M, Pallini C, Pike JA, Perrella G, Quintanilla LG, Eble JA, Poulter NS, Heemskerk JW, Watson SP (2020) Comparison of the GPVI inhibitors losartan and honokiol. Platelets 31(2):187–197
Pastori D, Cormaci VM, Marucci S, Franchino G, Del Sole F, Capozza A, Fallarino A, Corso C, Valeriani E, Menichelli D (2023) A comprehensive review of risk factors for venous thromboembolism: from epidemiology to pathophysiology. Int J Mol Sci 24(4):3169
Paul BZ, Daniel JL, Kunapuli SP (1999) Platelet shape change is mediated by both calcium-dependent and-independent signaling pathways: role of p160 Rho-associated coiled-coil-containing protein kinase in platelet shape change. J Biol Chem 274(40):28293–28300
Paul M, Paul JW, Hinwood M, Hood RJ, Martin K, Abdolhoseini M, Johnson SJ, Pollack M, Nilsson M, Walker FR (2023) Clopidogrel administration impairs post-stroke learning and memory recovery in mice. Int J Mol Sci 24(14):11706
Pennings GJ, Reddel CJ, Chen VM, Gnanenthiran SR, Kritharides L (2023) Perspective: collagen induced platelet activation via the GPVI receptor as a primary target of colchicine in cardiovascular disease. Front Cardiovasc Med 9:1104744
Perrella G, Montague SJ, Brown HC, Garcia Quintanilla L, Slater A, Stegner D, Thomas M, Heemskerk JW, Watson SP (2022) Role of tyrosine kinase Syk in thrombus stabilisation at high shear. Int J Mol Sci 23(1):493
Piskin S, Uzunali E (2007) A review of the use of adapalene for the treatment of acne vulgaris. Ther Clin Risk Manag 3(4):621–624
Prajapati C, Tripathi PN, Sood S, Rai SN, Mishra SS, Singh SK, Tiwari AK (2025) Intellectual property rights in neuroprotective biomaterials. In: Biomaterials and neurodegenerative disorders. Springer, pp 251–269
Qutub AA, Popel AS (2008) Reactive oxygen species regulate hypoxia-inducible factor 1α differentially in cancer and ischemia. Mol Cell Biol 28(16):5106–5119
Rai SN, Singh S, Singh SK (2024) Neurodegenerative diseases: translational models, mechanisms, and therapeutics. CRC Press

Rai SN (2021) Recent advances in the treatment of neurodegenerative disorders.
Ramakrishna K, Singh N, Krishnamurthy S (2022a) Diindolylmethane ameliorates platelet aggregation and thrombosis: in silico, in vitro, and in vivo studies. Eur J Pharmacol 919:174812
Ramakrishna K, Singh SK, Krishnamurthy S (2022b) Diindolylmethane ameliorates ischemic stroke-induced brain injury by peripheral and central mechanisms. Curr Neurovasc Res 19(5):462–475
Ramakrishna K, Viswanadh MK, Dumala N, Chakravarth G, Venkateswarlu K, Gutti G, Yadagiri G, Duguluri S, Rai SN (2025) Advanced biomaterials in neuroprotection: innovations and clinical applications. In: Biomaterials and neurodegenerative disorders. Springer, pp 69–92
Rayner-Hartley E, Sedlak T (2016) Ranolazine: a contemporary review. J Am Heart Assoc 5(3):e003196
Reddy BM, Weintraub HS, Schwartzbard AZ (2010) Ranolazine: a new approach to treating an old problem. Tex Heart Inst J 37(6):641
Rele S, Thakur CK, Khan F, Baral B, Saini V, Karthikeyan C, Moorthy NHN, Jha HC (2024) Curcumin coating: a novel solution to mitigate inherent carbon nanotube toxicity. J Mater Sci - Mater Med 35(1):24
Roy S, Dhaneshwar S, Bhasin B (2021) Drug repurposing: an emerging tool for drug reuse, recycling and discovery. Current Drug Res Rev Formerly: Curr Drug Abuse Rev 13(2):101–119
Rusu A, Tanase C, Pascu G-A, Todoran N (2020) Recent advances regarding the therapeutic potential of adapalene. Pharmaceuticals 13(9):217
Sakata C, Kawasaki T, Kato Y, Abe M, Suzuki K-i, Ohmiya M, Funatsu T, Morita Y, Okada M (2013) ASP6537, a novel highly selective cyclooxygenase-1 inhibitor, exerts potent antithrombotic effect without "aspirin dilemma." Thromb Res 132(1):56–62
Samir SM, Hassan HM, Elmowafy R, ElNashar EM, Alghamdi MA, AlSheikh MH, Al-Zahrani NS, Alasiri FM, Elhadidy MG (2024) Neuroprotective effect of ranolazine improves behavioral discrepancies in a rat model of scopolamine-induced dementia. Front Neurosci 17:1267675
Saraf P, Tripathi PN, Tripathi MK, Tripathi A, Verma H, Waiker DK, Singh R, Shrivastava SK (2022) Novel 5, 6-diphenyl-1, 2, 4-triazine-3-thiol derivatives as dual COX-2/5-LOX inhibitors devoid of cardiotoxicity. Bioorg Chem 129:106147
Saver JL (2006) Time is brain—quantified. Stroke 37(1):263–266
Sharma A (2016) Neuroprotective agents. In: Advances in structure and activity relationship of coumarin derivatives. Elsevier, pp 77–99
Shen X, Li M, Shao K, Li Y, Ge Z (2023) Post-ischemic inflammatory response in the brain: targeting immune cell in ischemic stroke therapy. Front Mol Neurosci 16:1076016
Shibata S, Sakurai K, Tachikawa K, Ko R, Hino S, Fukano T, Isahaya K, Haraguchi T, Yamauchi J, Tanabe K (2022) The utility of automated ASPECTS in acute ischemic stroke for intravenous recombinant tissue plasminogen activator (IV-rtPA) therapy. Neurol Int 14(4):981–990
Singh A, Saini R, Mishra A (2022) Novel allosteric inhibitor to target drug resistance in EGFR mutant: molecular modelling and free energy approach. Mol Simul 48(9):801–811
Singh S, Rai SN, Singh SK (2024) Synaptic plasticity in neurodegenerative disorders. CRC Press
Song J, Miermont A, Lim CT, Kamm RD (2018) A 3D microvascular network model to study the impact of hypoxia on the extravasation potential of breast cell lines. Sci Rep 8(1):17949
Su F, Yang H, Guo A, Qu Z, Wu J, Wang Q (2021) Mitochondrial BKCa mediates the protective effect of low-dose ethanol preconditioning on oxygen-glucose deprivation and reperfusion-induced neuronal apoptosis. Front Physiol 12:719753
Swan D, Loughran N, Makris M, Thachil J (2020) Management of bleeding and procedures in patients on antiplatelet therapy. Blood Rev 39:100619
Tambuwala MM, Khan MN, Thompson P, McCarron PA (2019) Albumin nano-encapsulation of caffeic acid phenethyl ester and piceatannol potentiated its ability to modulate HIF and NF-kB pathways and improves therapeutic outcome in experimental colitis. Drug Deliv Transl Res 9:14–24
Taylor L, Vasudevan SR, Jones CI, Gibbins JM, Churchill GC, Campbell RD, Coxon CH (2014) Discovery of novel GPVI receptor antagonists by structure-based repurposing. PLoS ONE 9(6):e101209
Tomaiuolo M, Brass LF, Stalker TJ (2017) Regulation of platelet activation and coagulation and its role in vascular injury and arterial thrombosis. Interv Cardiol Clin 6(1):1
Tripathi P, Ganeshpurkar A, Singh SK, Krishnamurthy S (2023) Identification of novel glucocerebrosidase chaperone for potential treatment of Parkinson's disease: an approach using in silico virtual screening, molecular docking and molecular dynamics, and in vitro studies. Int J Biol Macromol 228:453–466
Tudor DV, Bâldea I, Olteanu DE, Fischer-Fodor E, Piroska V, Lupu M, Călinici T, Decea RM, Filip GA (2021) Celecoxib as a valuable adjuvant in cutaneous melanoma treated with trametinib. Int J Mol Sci 22(9):4387
Uğuz AC, Öz A, Yilmaz B, Altunbaş S, Çelik Ö (2015) Melatonin attenuates apoptosis and mitochondrial depolarization levels in hypoxic conditions of SH-SY5Y neuronal cells induced by cobalt chloride (CoCl2). Turk J Biol 39(6):896–903
Vaidya A, Wolska N, Vara D, Mailer R, Schröder K, Pula G (2021) Diabetes and Thrombosis: A Central Role for Vascular Oxidative Stress. Antioxidants 2021, 10, 706. s Note: MDPI stays neutral with regard to jurisdictional claims in published.
Vismara M (2021) Blood platelets and cancer: the involvement of platelet-derived extracellular vesicles in tumour progression.
Wei R, Song L, Miao Z, Liu K, Han G, Zhang H, Ma D, Huang J, Tian H, Xiao B (2022) Hydroxysafflor yellow a exerts neuroprotective effects via HIF-1α/BNIP3 pathway to activate neuronal autophagy after OGD/R. Cells 11(23):3726
Williams S, Pourrier M, McAfee D, Lin S, Fedida D (2014) Ranolazine improves diastolic function in spontaneously hypertensive rats. Am J Physiol-Heart Circulat Physiol 306(6):H867–H881
Wu L, Xiong X, Wu X, Ye Y, Jian Z, Zhi Z, Gu L (2020a) Targeting oxidative stress and inflammation to prevent ischemia-reperfusion injury. Front Mol Neurosci 13:28
Wu Q-L, Dong J, Zeng H-W, Lv C, Liu A-J, Zhang W-D (2020b) Monitoring antiplatelet aggregation in vivo and in vitro by microtiter plate method. J Cardiovasc Pharmacol 75(4):314–320
Yang M, Huo X, Miao Z, Wang Y (2019) Platelet glycoprotein IIb/IIIa receptor inhibitor tirofiban in acute ischemic stroke. Drugs 79(5):515–529
Yeung J, Holinstat M (2012) Newer agents in antiplatelet therapy: a review. J Blood Med. https://doi.org/10.2147/JBM.S25421
Yin H, Litvinov RI, Vilaire G, Zhu H, Li W, Caputo GA, Moore DT, Lear JD, Weisel JW, DeGrado WF (2006) Activation of platelet αIIbβ3 by an exogenous peptide corresponding to the transmembrane domain of αIIb. J Biol Chem 281(48):36732–36741
Yu Y, Li W, Ren L, Yang C, Li D, Han X, Sun Y, Lv C, Han F (2018) Inhibition of autophagy enhanced cobalt chloride-induced apoptosis in rat alveolar type II epithelial cells. Mol Med Rep 18(2):2124–2132
Yu S, Xiong W, Xu W, Chen Y (2024) Heliox protects SH-SY5Y cells from oxygen-glucose deprivation/reperfusion-induced ferroptosis. J Integr Neurosci 23(1):14
Zhang M, Ma Y, Fan X (2019) Storax protected oxygen-glucose deprivation/reoxygenation induced primary astrocyte injury by inhibiting NF-κB activation in vitro. Front Pharmacol 9:419703
Zhou Y, Hu Y, Lu X, Yang H, Li Q, Du C, Chen Y, Hong KH, Sun H (2020) Discovery of a selective 6-hydroxy-1, 4-diazepan-2-one containing butyrylcholinesterase inhibitor by

virtual screening and MM-GBSA rescoring. Dose-Response 18(2):1559325820938526
Zimran A, Elstein D (2003) Gaucher disease and the clinical experience with substrate reduction therapy. Philos Trans R Soc Lond B Biol Sci 358(1433):961–966
Zyubin A, Rafalskiy V, Tcibulnikova A, Matveeva K, Moiseeva E, Tsapkova A, Samusev I, Bryukhanov V, Demin M (2020) Dataset of human platelets in healthy and individuals with cardiovascular pathology obtained by surface-enhanced Raman spectroscopy. Data Brief 29:105145

Authors and Affiliations

Mohammad Aquib Siddiqui[1] · Poorvi Saraf[2] · Sushant Kumar Shrivastava[2] · Sudha Madhavi Penumaka[3] · Debabrata Mandal[3] · Ravi Saini[4] · Abhishek Pathak[5] · Kakarla Ramakrishna[6] · Sairam Krishnamurthy[1]

✉ Sairam Krishnamurthy
ksairam.phe@iitbhu.ac.in

Mohammad Aquib Siddiqui
mdaquib.siddiqui.rs.phe18@itbhu.ac.in

Poorvi Saraf
Poorvisaraf.rs.phe19@itbhu.ac.in

Sushant Kumar Shrivastava
Skshrivastava.phe@itbhu.ac.in

Sudha Madhavi Penumaka
madhavi47penumaka@gmail.com

Debabrata Mandal
dmandal@niperhajipur.ac.in

Ravi Saini
ravisaini.rs.bce18@iitbhu.ac.in

Abhishek Pathak
abhishekpathakaiims@gmail.com

Kakarla Ramakrishna
kakarlaramakrishna@kluniversity.in

1 Neurotherapeutics Research Laboratory, Department of Pharmaceutical Engineering and Technology, Indian Institute of Technology (Banaras Hindu University), Varanasi 221005, India

2 Pharmaceutical Chemistry Research Laboratory, Department of Pharmaceutical Engineering and Technology, Indian Institute of Technology (Banaras Hindu University), Varanasi 221005, India

3 Department of Biotechnology, National Institute of Pharmaceutical Education and Research, Hajipur 844102, India

4 School of Biochemical Engineering, Indian Institute of Technology (Banaras Hindu University), Varanasi 221005, India

5 Department of Neurology, Institute of Medical Science (IMS), Banaras Hindu University, Varanasi 221005, India

6 KL College of Pharmacy, Koneru Lakshmaiah Education Foundation, Vaddeswaram 522302, India